EUROPEAN LABORATORY FOR PARTICLE PHYSICS (CERN)

CERN-EP/99-014
February 5th, 1999

Search for Charginos and Neutralinos in e^+e^- Collisions at Centre-of-Mass Energies near 183 GeV and Constraints on the MSSM Parameter Space

The ALEPH Collaboration*)

Abstract

Searches for charginos and neutralinos are performed with the data collected by the ALEPH detector at LEP at centre-of-mass energies near 183 GeV. In these searches, it is assumed that R-parity is conserved and that the lightest neutralino is the LSP. No evidence of a signal is observed in the $57\,\mathrm{pb}^{-1}$ accumulated, which excludes chargino and associated neutralino production up to the kinematic limit over large regions of the MSSM parameter space. Under the assumptions of common gaugino and common sfermion masses at the unification scale, the interplay between the chargino, neutralino and slepton exclusions allows a lower limit of $27\,\mathrm{GeV}/c^2$ to be set on the mass of the lightest neutralino. Tighter constraints on the MSSM parameter space are obtained using in addition exclusions in the Higgs sector. Finally, the results are interpreted within the framework of minimal supergravity.

(To be submitted to European Physics Journal)

---

*) See next pages for the list of authors

The ALEPH Collaboration

R. Barate, D. Decamp, P. Ghez, C. Goy, S. Jezequel, J.-P. Lees, F. Martin, E. Merle, M.-N. Minard, J.-Y. Nief, B. Pietrzyk

Laboratoire de Physique des Particules (LAPP), IN^{2}P^3-CNRS, F-74019 Annecy-le-Vieux Cedex, France

R. Alemany, M.P. Casado, M. Chmeissani, J.M. Crespo, M. Delfino, E. Fernandez, M. Fernandez-Bosman, Ll. Garrido,[15] E. Graugès, A. Juste, M. Martinez, G. Merino, R. Miquel, Ll.M. Mir, P. Morawitz, A. Pacheco, I.C. Park, A. Pascual, I. Riu, F. Sanchez

Institut de Física d'Altes Energies, Universitat Autònoma de Barcelona, 08193 Bellaterra (Barcelona), E-Spain[7]

A. Colaleo, D. Creanza, M. de Palma, G. Gelao, G. Iaselli, G. Maggi, M. Maggi, S. Nuzzo, A. Ranieri, G. Raso, F. Ruggieri, G. Selvaggi, L. Silvestris, P. Tempesta, A. Tricomi,[3] G. Zito

Dipartimento di Fisica, INFN Sezione di Bari, I-70126 Bari, Italy

X. Huang, J. Lin, Q. Ouyang, T. Wang, Y. Xie, R. Xu, S. Xue, J. Zhang, L. Zhang, W. Zhao

Institute of High-Energy Physics, Academia Sinica, Beijing, The People's Republic of China[8]

D. Abbaneo, U. Becker,[22] G. Boix,[2] M. Cattaneo, V. Ciulli, G. Dissertori, H. Drevermann, R.W. Forty, M. Frank, F. Gianotti, A.W. Halley, J.B. Hansen, J. Harvey, P. Janot, B. Jost, I. Lehraus, O. Leroy, C. Loomis, P. Maley, P. Mato, A. Minten, A. Moutoussi, F. Ranjard, L. Rolandi, D. Rousseau, D. Schlatter, M. Schmitt,[12] O. Schneider,[23] W. Tejessy, F. Teubert, I.R. Tomalin, E. Tournefier, M. Vreeswijk, A.E. Wright

European Laboratory for Particle Physics (CERN), CH-1211 Geneva 23, Switzerland

Z. Ajaltouni, F. Badaud G. Chazelle, O. Deschamps, S. Dessagne, A. Falvard, C. Ferdi, P. Gay, C. Guicheney, P. Henrard, J. Jousset, B. Michel, S. Monteil, J-C. Montret, D. Pallin, P. Perret, F. Podlyski

Laboratoire de Physique Corpusculaire, Université Blaise Pascal, IN^{2}P^3-CNRS, Clermont-Ferrand, F-63177 Aubière, France

J.D. Hansen, J.R. Hansen, P.H. Hansen, B.S. Nilsson, B. Rensch, A. Wäänänen

Niels Bohr Institute, 2100 Copenhagen, DK-Denmark[9]

G. Daskalakis, A. Kyriakis, C. Markou, E. Simopoulou, A. Vayaki

Nuclear Research Center Demokritos (NRCD), GR-15310 Attiki, Greece

A. Blondel, J.-C. Brient, F. Machefert, A. Rougé, M. Swynghedauw, R. Tanaka, A. Valassi,[6] H. Videau

Laboratoire de Physique Nucléaire et des Hautes Energies, Ecole Polytechnique, IN^{2}P^3-CNRS, F-91128 Palaiseau Cedex, France

E. Focardi, G. Parrini, K. Zachariadou

Dipartimento di Fisica, Università di Firenze, INFN Sezione di Firenze, I-50125 Firenze, Italy

R. Cavanaugh, M. Corden, C. Georgiopoulos

Supercomputer Computations Research Institute, Florida State University, Tallahassee, FL 32306-4052, USA [13,14]

A. Antonelli, G. Bencivenni, G. Bologna,[4] F. Bossi, P. Campana, G. Capon, F. Cerutti, V. Chiarella, P. Laurelli, G. Mannocchi,[5] F. Murtas, G.P. Murtas, L. Passalacqua, M. Pepe-Altarelli[1]

Laboratori Nazionali dell'INFN (LNF-INFN), I-00044 Frascati, Italy

M. Chalmers, L. Curtis, J.G. Lynch, P. Negus, V. O'Shea, B. Raeven, C. Raine, D. Smith, P. Teixeira-Dias, A.S. Thompson, J.J. Ward

Department of Physics and Astronomy, University of Glasgow, Glasgow G12 8QQ,United Kingdom[10]

O. Buchmüller, S. Dhamotharan, C. Geweniger, P. Hanke, G. Hansper, V. Hepp, E.E. Kluge, A. Putzer, J. Sommer, K. Tittel, S. Werner,[22] M. Wunsch

Institut für Hochenergiephysik, Universität Heidelberg, D-69120 Heidelberg, Germany[16]

R. Beuselinck, D.M. Binnie, W. Cameron, P.J. Dornan,[1] M. Girone, S. Goodsir, N. Marinelli, E.B. Martin, J. Nash, J. Nowell, J.K. Sedgbeer, P. Spagnolo, E. Thomson, M.D. Williams

Department of Physics, Imperial College, London SW7 2BZ, United Kingdom[10]

V.M. Ghete, P. Girtler, E. Kneringer, D. Kuhn, G. Rudolph

Institut für Experimentalphysik, Universität Innsbruck, A-6020 Innsbruck, Austria[18]

A.P. Betteridge, C.K. Bowdery, P.G. Buck, P. Colrain, G. Crawford, G. Ellis, A.J. Finch, F. Foster, G. Hughes, R.W.L. Jones, N.A. Robertson, M.I. Williams

Department of Physics, University of Lancaster, Lancaster LA1 4YB, United Kingdom[10]

P. van Gemmeren, I. Giehl, F. Hölldorfer, C. Hoffmann, K. Jakobs, K. Kleinknecht, M. Kröcker, H.-A. Nürnberger, G. Quast, B. Renk, E. Rohne, H.-G. Sander, S. Schmeling, H. Wachsmuth C. Zeitnitz, T. Ziegler

Institut für Physik, Universität Mainz, D-55099 Mainz, Germany[16]

J.J. Aubert, C. Benchouk, A. Bonissent, J. Carr,[1] P. Coyle, A. Ealet, D. Fouchez, F. Motsch, P. Payre, M. Talby, M. Thulasidas, A. Tilquin

Centre de Physique des Particules, Faculté des Sciences de Luminy, IN^{2}P^3-CNRS, F-13288 Marseille, France

M. Aleppo, M. Antonelli, F. Ragusa

Dipartimento di Fisica, Università di Milano e INFN Sezione di Milano, I-20133 Milano, Italy.

R. Berlich, V. Büscher, H. Dietl, G. Ganis, K. Hüttmann, G. Lütjens, C. Mannert, W. Männer, H.-G. Moser, S. Schael, R. Settles, H. Seywerd, H. Stenzel, W. Wiedenmann, G. Wolf

Max-Planck-Institut für Physik, Werner-Heisenberg-Institut, D-80805 München, Germany[16]

P. Azzurri, J. Boucrot, O. Callot, S. Chen, M. Davier, L. Duflot, J.-F. Grivaz, Ph. Heusse, A. Jacholkowska, M. Kado, J. Lefrançois, L. Serin, J.-J. Veillet, I. Videau,[1] J.-B. de Vivie de Régie, D. Zerwas

Laboratoire de l'Accélérateur Linéaire, Université de Paris-Sud, IN^{2}P^3-CNRS, F-91898 Orsay Cedex, France

G. Bagliesi, S. Bettarini, T. Boccali, C. Bozzi, G. Calderini, R. Dell'Orso, I. Ferrante, A. Giassi, A. Gregorio, F. Ligabue, A. Lusiani, P.S. Marrocchesi, A. Messineo, F. Palla, G. Rizzo, G. Sanguinetti, A. Sciabà, G. Sguazzoni, R. Tenchini, C. Vannini, A. Venturi, P.G. Verdini

Dipartimento di Fisica dell'Università, INFN Sezione di Pisa, e Scuola Normale Superiore, I-56010 Pisa, Italy

G.A. Blair, J. Coles, G. Cowan, M.G. Green, D.E. Hutchcroft, L.T. Jones, T. Medcalf, J.A. Strong, J.H. von Wimmersperg-Toeller

Department of Physics, Royal Holloway & Bedford New College, University of London, Surrey TW20 OEX, United Kingdom[10]

D.R. Botterill, R.W. Clifft, T.R. Edgecock, P.R. Norton, J.C. Thompson

Particle Physics Dept., Rutherford Appleton Laboratory, Chilton, Didcot, Oxon OX11 OQX, United Kingdom[10]

B. Bloch-Devaux, P. Colas, B. Fabbro, G. Faïf, E. Lançon, M.-C. Lemaire, E. Locci, P. Perez, H. Przysiezniak, J. Rander, J.-F. Renardy, A. Rosowsky, A. Trabelsi,[20] B. Tuchming, B. Vallage

CEA, DAPNIA/Service de Physique des Particules, CE-Saclay, F-91191 Gif-sur-Yvette Cedex, France[17]

S.N. Black, J.H. Dann, H.Y. Kim, N. Konstantinidis, A.M. Litke, M.A. McNeil, G. Taylor

Institute for Particle Physics, University of California at Santa Cruz, Santa Cruz, CA 95064, USA[19]

C.N. Booth, S. Cartwright, F. Combley, P.N. Hodgson, M.S. Kelly, M. Lehto, L.F. Thompson
Department of Physics, University of Sheffield, Sheffield S3 7RH, United Kingdom[10]

K. Affholderbach, A. Böhrer, S. Brandt, C. Grupen, A. Misiejuk, G. Prange, U. Sieler
Fachbereich Physik, Universität Siegen, D-57068 Siegen, Germany[16]

G. Giannini, B. Gobbo
Dipartimento di Fisica, Università di Trieste e INFN Sezione di Trieste, I-34127 Trieste, Italy

J. Putz, J. Rothberg, S. Wasserbaech, R.W. Williams
Experimental Elementary Particle Physics, University of Washington, WA 98195 Seattle, U.S.A.

S.R. Armstrong, E. Charles, P. Elmer, D.P.S. Ferguson, Y. Gao, S. González, T.C. Greening, O.J. Hayes, H. Hu, S. Jin, P.A. McNamara III, J.M. Nachtman,[21] J. Nielsen, W. Orejudos, Y.B. Pan, Y. Saadi, I.J. Scott, J. Walsh, Sau Lan Wu, X. Wu, G. Zobernig
Department of Physics, University of Wisconsin, Madison, WI 53706, USA[11]

[1]Also at CERN, 1211 Geneva 23, Switzerland.
[2]Supported by the Commission of the European Communities, contract ERBFMBICT982894.
[3]Also at Dipartimento di Fisica, INFN Sezione di Catania, 95129 Catania, Italy.
[4]Also Istituto di Fisica Generale, Università di Torino, 10125 Torino, Italy.
[5]Also Istituto di Cosmo-Geofisica del C.N.R., Torino, Italy.
[6]Now at LAL, 91898 Orsay, France.
[7]Supported by CICYT, Spain.
[8]Supported by the National Science Foundation of China.
[9]Supported by the Danish Natural Science Research Council.
[10]Supported by the UK Particle Physics and Astronomy Research Council.
[11]Supported by the US Department of Energy, grant DE-FG0295-ER40896.
[12]Now at Harvard University, Cambridge, MA 02138, U.S.A.
[13]Supported by the US Department of Energy, contract DE-FG05-92ER40742.
[14]Supported by the US Department of Energy, contract DE-FC05-85ER250000.
[15]Permanent address: Universitat de Barcelona, 08208 Barcelona, Spain.
[16]Supported by the Bundesministerium für Bildung, Wissenschaft, Forschung und Technologie, Germany.
[17]Supported by the Direction des Sciences de la Matière, C.E.A.
[18]Supported by Fonds zur Förderung der wissenschaftlichen Forschung, Austria.
[19]Supported by the US Department of Energy, grant DE-FG03-92ER40689.
[20]Now at Département de Physique, Faculté des Sciences de Tunis, 1060 Le Belvédère, Tunisia.
[21]Now at University of California at Los Angeles (UCLA), Los Angeles, CA 90024, U.S.A.
[22]Now at SAP AG, 69185 Walldorf, Germany
[23]Now at Université de Lausanne, 1015 Lausanne, Switzerland.

1 Introduction

In 1997, the ALEPH detector at LEP collected an integrated luminosity of $57\,\mathrm{pb}^{-1}$ in $\mathrm{e}^+\mathrm{e}^-$ collisions at centre-of-mass energies near 183 GeV. This increased energy allowed searches for the new states predicted by supersymmetric models [1] to be performed in an as yet unexplored domain. Signals of scalar leptons [2] or scalar quarks [3] were not observed, and mass lower limits have been set. In this paper, searches for charginos and neutralinos, the supersymmetric partners of the gauge and Higgs bosons, are reported. The data sample, hereafter referred to as *the 183 GeV data*, consists of $0.2\,\mathrm{pb}^{-1}$ collected at 180.8 GeV, $3.9\,\mathrm{pb}^{-1}$ at 181.7 GeV, $50.9\,\mathrm{pb}^{-1}$ at 182.7 GeV and $1.9\,\mathrm{pb}^{-1}$ at 183.8 GeV. The analyses are conducted within the framework of the minimal supersymmetric extension of the standard model (MSSM) with R-parity conservation. The lightest neutralino χ is assumed to be the lightest supersymmetric particle (LSP); it is neutral, stable, and weakly interacting, and therefore escapes detection.

Standard notations and conventions are used for the MSSM parameters, as detailed in Ref. [4]. The unification relation $M_1 = \frac{5}{3} M_2 \tan^2\theta_W$ among the gaugino SUSY breaking mass terms is assumed throughout. The region where $M_2 \gg |\mu|$ is referred to as the *higgsino region*, and the region where $|\mu| \gg M_2$ as the *gaugino region*. In the higgsino region, the lightest neutralino χ is close in mass to the lightest chargino $\chi^\pm$, while in the gaugino region $m_\chi \sim m_{\chi^\pm}/2$. The region of small negative μ and low M_2 is referred to as the *mixed region*.

Charginos ($\chi^\pm$,$\chi_2^\pm$) are pair produced in the s channel via photon and Z exchange and in the t channel via sneutrino exchange, with destructive interference between the s and the t terms. As a consequence, lighter sneutrinos are associated with a lower production cross section. In most cases charginos decay to the lightest neutralino and a fermion anti-fermion pair via W, slepton, and squark exchange.

Neutralinos (χ,χ',χ'',χ''') are pair produced in the s channel via Z exchange and in the t channel via selectron exchange, with constructive interference between the s and the t terms. Neutralino cross sections are therefore larger if selectrons are lighter. In most cases neutralinos decay to a lighter neutralino and a fermion anti-fermion pair via Z, slepton, and squark exchange. In the higgsino region, $\chi\chi'$ is the only relevant neutralino production process. In the mixed region, the heavier neutralinos (χ'', χ''') can also be produced. They decay through cascades to the lighter neutralinos, thus giving rise to complex topologies. In this same region the radiative decay $\chi' \to \chi\gamma$ has a sizeable branching ratio.

The main features which affect the final state topologies are the difference in mass between the produced particles and the LSP, and the leptonic decay branching ratios. As in Ref. [4], a large number of selections is used to cope with the various possibilities. After a brief description of the ALEPH detector in Section 2, an overview of these selections is given in Section 3. The detailed descriptions of the selection variables and criteria are deferred to Appendices.

The chargino-neutralino mass spectrum is entirely determined by the parameters M_2, μ and $\tan\beta$. Except when all sfermions are sufficiently heavy, detailed information as to the sfermion mass spectrum is needed to specify the various production cross sections and decay

branching ratios. For this purpose, a common SUSY breaking mass m_0 is assumed for all sleptons and squarks at the grand unification scale, and the renormalization group equations are used to determine the low energy parameters.

Cross section upper limits for chargino and neutralino production are first extracted from the data. Excluded domains in the MSSM parameter space are then determined, and limits on the masses of charginos and neutralinos, in particular of the lightest one, are inferred. The influence of $\tan\beta$ and m_0 on the LSP mass lower limit is investigated, and a limit independent of $\tan\beta$ and m_0 is obtained. These results are presented in Section 4. Constraints on the MSSM parameter space inferred from Higgs boson searches [5] are also discussed in Section 4. Finally, an interpretation of all supersymmetric particle and Higgs boson searches performed by ALEPH is presented in that same section within the framework of minimal supergravity [6], *i.e*, assuming unification of Higgs boson and sfermion masses and radiative electroweak symmetry breaking. A comprehensive summary of all results is given in Section 5.

2 The ALEPH Detector

A thorough description of the ALEPH detector can be found in Refs. [7, 8], and an account of its performance as well as a description of the standard analysis algorithms in Ref. [9].

Briefly, the tracking system consists of a silicon vertex detector, a cylindrical drift chamber, and a large time projection chamber, all immersed in a 1.5 T magnetic field provided by a superconducting solenoidal coil. This ensemble allows a charged particle $1/p_T$ resolution of $(6 \times 10^{-4} \oplus 5 \times 10^{-3}/p_T)$ $(\mathrm{GeV}/c)^{-1}$ to be achieved.

Between the tracking system and the coil, a highly granular electromagnetic calorimeter is used to identify electrons and photons and to measure their energy with a relative resolution of $0.18/\sqrt{E} + 0.009$ (E in GeV). It is complemented at low angles by luminosity calorimeters. The iron return yoke is instrumented to act as a hadron calorimeter. It provides a measurement of the hadronic energy with a relative resolution of $0.85/\sqrt{E}$ (E in GeV) and, together with external chambers, allows muon identification. Altogether, the calorimetric coverage is hermetic down to 34 mrad of the beam axis.

The information from all these detectors is combined in an energy flow algorithm which provides a list of *particles*, categorized as charged particles, photons, and neutral hadrons. These particles are used in all the analyses which follow, in particular to determine global quantities such as total energy or missing momentum. The resolution achieved on the total energy is $(0.6\sqrt{E} + 0.6)$ GeV (E in GeV).

The relevant trigger conditions are highly redundant and fully efficient for the simulated signal events accepted by the selection criteria described in the next section.

3 Searches for Charginos and Neutralinos

If all sfermions are substantially heavier than the W and Z bosons, charginos and neutralinos decay via W and Z exchange, respectively. In this case, chargino searches are performed in the four-jet topology (4J) and in a topology with hadrons plus an isolated electron or muon (2Jℓ) as in Ref. [4]. New analyses are introduced to cover the case where the lepton is a tau (2Jτ). In the higgsino region, $\chi\chi'$ production and decay lead to a dominant acoplanar jet topology (AJ). In the mixed region, cascade decays of the heavier neutralinos and radiative decays of χ' are selected by a multihadron–plus–photon analysis (4Jγ).

The properties of the decay products are mainly governed by the mass difference ΔM between the decaying particle and the lightest neutralino. For small ΔM (typical of the higgsino region) the phase space for the decay is small and the signal topology resembles that of $\gamma\gamma \to$ hadrons events, whereas for large ΔM (typical of the gaugino and mixed regions) the signal topology is closer to that of four-fermion final states originating from, *e.g.*, WW and ZZ production. The very low (VL), low (L), high (H) and very high (VH) ΔM regions are addressed by different selections.

If sleptons are light, leptonic decays of charginos and neutralinos are enhanced due to the increased influence of slepton exchange diagrams. The dominant topology consists of an acoplanar lepton pair (Aℓ). When sleptons are light enough, two-body decays such as $\chi^{\pm} \to \ell\tilde{\nu}$, $\chi' \to \ell\tilde{\ell}$, and the invisible $\chi' \to \nu\tilde{\nu}$ become kinematically allowed. In the mixed region, production and cascade decays of the heavier neutralinos give rise to final states containing many leptons. These topologies are covered by a dedicated multilepton analysis (Mℓ).

The chargino and neutralino selections are similar to those developed for the 161 and 172 GeV data [4]. Only a general description of the search strategy and optimization as well as the most important cuts are given here. Details can be found in Appendix A, where the variables are described, and Appendix B, where the various selections are detailed.

The selection criteria are optimized according to the $\overline{N}_{95}$ prescription, *i.e.*, by minimizing the expected 95% C.L. cross section upper limit in the absence of signal, determined from Monte Carlo simulations [10]. Except for the Aℓ selections, no background subtraction is performed. The selections are optimized for several ΔM values. Some cut values, hereafter referred to as sliding cuts, are parametrized as a function of ΔM. With this method, events contribute only for the precise ΔM values with which they are consistent.

Due to the difficulty to simulate the $\gamma\gamma \to$ hadrons background accurately, a specific procedure is used to reject this background, as discussed in Ref. [4]. Energy-based and direction-based variables are used in conjunction. The resulting anti-$\gamma\gamma$ cuts are more stringent than would be required by the $\overline{N}_{95}$ prescription. For optimization purposes, an event rejected by a single cut still counts as a fraction of an event, with a weight depending on its distance from the cut value. In the case of the very low ΔM selections, where $\gamma\gamma \to$ hadrons is the main background, all criteria are optimized simultaneously according to this prescription. For the other selections, the optimization is aimed at the reduction of the other backgrounds, and the anti-$\gamma\gamma$ cuts are only allowed to be tightened.

3.1 Monte Carlo Samples

The signal events were generated with SUSYGEN [11], which simulates chargino and neutralino production, including cascade decays and two- and three-body decays as well as final state radiation.

Standard Model processes were simulated with

- UNIBAB [12] for Bhabha production;
- KORALZ [13] for $\mu^+\mu^-$ and $\tau^+\tau^-$ production;
- PHOT02 [14] for $\gamma\gamma \to$ leptons events and tagged $\gamma\gamma \to$ hadrons events;
- PHOJET [15] for untagged $\gamma\gamma \to$ hadrons events;
- KORALW [16] for WW events;
- PYTHIA [17] for all other processes.

The simulated samples correspond to at least 15 times the integrated luminosity of the data, except for $\gamma\gamma \to$ hadrons where the factor is five. The $\gamma\gamma \to$ hadrons events were generated with hadronic masses in excess of $2.5\,\mathrm{GeV}/c^2$. All standard model background samples were processed through the full detector simulation as well as the signal samples for charginos close to the kinematic limit. For the other samples of chargino events and for the neutralino event samples, a fast simulation was used. This fast simulation was cross-checked with several fully simulated samples.

3.2 Chargino selections

For a given ΔM value, the 2Jℓ selections, which are always relevant except for extreme values of the leptonic branching ratio, are optimized first. The 4J selections are optimized next, keeping the 2Jℓ selections unchanged and minimizing the expected cross section upper limit of the combined 2Jℓ and 4J selections for a signal with W* branching ratios. In a last step, the 2Jτ selections are optimized in a similar way, as additional to the 4J and 2Jℓ selections.

The chargino selections are designed for a particular range of ΔM values: H and VH for $\Delta M \simeq m_{\chi^\pm}/2$ and above, L for $\Delta M \simeq 20\,\mathrm{GeV}/c^2$, and VL for $\Delta M < 10\,\mathrm{GeV}/c^2$. Sliding cuts ensure smooth transitions between ΔM regions, but the choice of variables inherently limits the domain of applicability of any given selection.

The 4J and 2Jℓ analyses are similar to those described in Ref. [4], except for the introduction of sliding cuts. For the high ΔM analyses, the visible and hadronic energies are preferred to the visible and hadronic masses. Indeed, the main background arises from WW production in which the W's have a non-negligible boost at $\sqrt{s} \simeq 183\,\mathrm{GeV}$, while the optimization is aimed at charginos close to the kinematic limit (*i.e.*, with masses larger

than m_{W}). Cuts on the missing mass and on the energy of the leading lepton reduce the $\mathrm{WW} \to \ell\nu\mathrm{qq}$ background. The y_{cut} value y_{23} for which a given event, clustered with the Durham algorithm, changes from a two-jet to a three-jet topology is used to reject the $\mathrm{WW} \to \tau\nu\mathrm{qq}$ background in conjunction with the visible mass (hadronic energy) in the 4J (2Jℓ) analyses. As a side effect, the efficiency of the 4J selections on signal events with two jets and a τ is greatly reduced, and new analyses are introduced for those topologies. The 2Jτ selections are based on global kinematic quantities, *i.e.*, no attempt is made to reconstruct the τ jet. The background rejection is performed using the thrust, the visible energy, the visible mass, the missing mass, the acoplanarity and y_{23}.

The chargino selections for the very low ΔM region, which are quite sensitive to the $\gamma\gamma$ background, are improved with respect to those used at 161 and 172 GeV. The efficiency is increased by the lower value of the visible mass cut (3 GeV/c^2 instead of 4 GeV/c^2), which necessitated a redesign of the other cuts to maintain the background at a low level. The missing transverse momentum, the transverse acoplanarity and the missing mass are used to disentangle the signal from the $\gamma\gamma$ background. In the 2Jℓ-VL selection, the requirement of a lepton reduces the contamination from $\gamma\gamma \to$ hadrons, and cuts on the lepton transverse momentum and energy are used against the $\gamma\gamma \to \tau^+\tau^-$ background.

The Aℓ selections are used to cope with the cases where both charginos decay leptonically. The configuration where the sneutrino is lighter than the chargino is special. The relevant mass difference is $m_{\chi^\pm} - m_{\tilde{\nu}}$ rather than $m_{\chi^\pm} - m_{\chi}$ because the sneutrino is usually invisible. Hence, the acoplanar lepton chargino search is different in the case of three-body decays (Aℓ-3) and two-body decays to sneutrino (Aℓ-2). The topologies are very similar to $\mathrm{WW} \to \ell\nu\ell\nu$, except for the additional missing energy carried away by the two LSP's. These analyses are based on the searches for sleptons [2], but mixed lepton flavours are allowed. Cuts on the leading lepton energy are used to reject the WW background. In the case of Aℓ-2, the cut values are calculated from the chargino and sneutrino masses in order to select only the signal region; in the case of Aℓ-3, the sliding cut values are given in Appendix B. Final states with τ's suffer from large backgrounds; the $\ell\ell$, $\ell\tau$, and $\tau\tau$ topologies are therefore considered separately.

3.3 Neutralino selections

In the higgsino region, the only relevant neutralino production process is $\mathrm{e^+e^-} \to \chi\chi'$ which, in the MSSM, allows parameter configurations kinematically inaccessible to chargino pair production to be explored. The dominant decay mechanism is $\chi' \to \chi\mathrm{Z}^*$ because the higgsino components of χ and χ', responsible for their couplings to the Z, are large in that region. Acoplanar jets arising from the Z^* decay therefore constitute the main final state topology in the higgsino region.

Since the mass difference ΔM between the two neutralinos decreases when M_2 increases, two selections are designed for that region; the AJ-L selection, optimized for the low ΔM region (below 20 GeV/c^2), and the AJ-H selection, suited to the higher ΔM values. The optimization for the 183 GeV data leads to only one change with respect to the selections

applied at 161 and 172 GeV. For a more efficient rejection of the higher four-fermion background expected, the cut on the visible mass is replaced by a sliding cut on the missing mass. Indeed, since two massive χ's escape detection, the missing mass is expected to be large and increasing with decreasing ΔM, while four-fermion events generally have a smaller missing mass.

In the mixed region, additional production processes contribute such as $e^+e^- \to \chi'\chi'$ or $e^+e^- \to \chi\chi''$, with possible cascade decays of the heaviest neutralinos. The AJ-H selection still applies, but it is supplemented by a jets-plus-photon selection (4Jγ) to cope with the $\chi' \to \chi\gamma$ decay which may be sizeable in that region.

When sleptons are light, the leptonic branching ratios are enhanced through $\chi' \to \tilde{\ell}^*\ell \to \ell\ell\chi$. An acoplanar lepton or τ selection (Aℓ-χ), similar to that used for slepton searches [2], addresses the final states resulting from $\chi\chi'$ production. Same flavour leptons are required and the WW background is reduced by cuts on the lepton momenta. A selection of multileptonic final states (Mℓ), accompanied or not by hadrons, addresses the topologies resulting from $e^+e^- \to \chi'\chi'$ or from the production of heavier neutralinos. In the Mℓ selection, at least two electrons or two muons must be identified and the background is reduced by the use of sliding cuts on the lepton momenta and the visible mass.

3.4 Combination of selections

In the case of chargino production, the optimal combination of the 2Jℓ, 4J and 2Jτ selections is determined as a function of ΔM using samples of chargino events close to the kinematic limit and with $\chi^\pm \to W^*\chi$ decays. Combinations are defined in eight ΔM regions as summarized in Table 1. The corresponding efficiencies and total background are shown in Fig. 1.

As expected, each analysis is used in the ΔM region for which it is designed. One exception is the 2Jℓ-VL selection which suffers from a sizeable contamination from $\gamma\gamma$ interactions at low ΔM. However, for $\Delta M > 15\,\mathrm{GeV}/c^2$, the use of sliding cuts reduces the contamination to a negligible level while the efficiency remains substantial. This is why 2Jℓ-VL is also used in the range $15 < \Delta M < 25\,\mathrm{GeV}/c^2$ for which it is not optimized. The other exception is 4J-H which is not used for $\Delta M > 53\,\mathrm{GeV}/c^2$ because of its larger contamination from the WW and $q\overline{q}$ backgrounds compared to 2Jℓ-H.

The same eight ΔM regions are considered to address the case of sleptons light enough for leptonic decays to be enhanced, but still sufficiently heavy for two-body decays to be kinematically forbidden. In a given region, the optimal combination of the selections shown in Table 1 and of the chargino acoplanar lepton selections is determined as a function of the leptonic branching ratio. The leptonic branching ratio is varied by reweighting chargino events generated with $\chi^\pm \to W^*\chi$ decays. This procedure is applied only for mass differences typical of the gaugino and mixed regions since the branching ratios of charginos in the higgsino region are not very sensitive to the slepton masses. As a result, combinations are defined in regions of the (ΔM, BR_ℓ) plane (Table 2), where BR_ℓ is the chargino branching

Table 1: *Combinations of chargino selections as a function of ΔM for heavy sleptons.*

ΔM range	4J			2Jℓ			2Jτ		
(GeV/c^2)	H	L	VL	H	L	VL	VH	H	L
$\Delta M > 53$				$\surd$			$\surd$		
$36 < \Delta M < 53$	$\surd$			$\surd$			$\surd$	$\surd$	
$25 < \Delta M < 36$	$\surd$			$\surd$					$\surd$
$21 < \Delta M < 25$	$\surd$			$\surd$		$\surd$			$\surd$
$15 < \Delta M < 21$	$\surd$	$\surd$			$\surd$	$\surd$			
$9 < \Delta M < 15$	$\surd$	$\surd$			$\surd$				
$6 < \Delta M < 9$	$\surd$		$\surd$		$\surd$				
$\Delta M < 6$			$\surd$		$\surd$	$\surd$			

Table 2: *Combinations of chargino selections as a function of* BR_ℓ *for various* ΔM *ranges.*

$\Delta M > 53\,\mathrm{GeV}/c^2$				
BR_ℓ range	4J-H	2Jℓ-H	2Jτ-VH	$\ell\ell$-3
$\mathrm{BR}_\ell < 1\%$	$\surd$			
$1\% < \mathrm{BR}_\ell < 9\%$	$\surd$	$\surd$	$\surd$	
$9\% < \mathrm{BR}_\ell < 25\%$		$\surd$	$\surd$	
$25\% < \mathrm{BR}_\ell < 32\%$		$\surd$	$\surd$	$\surd$
$\mathrm{BR}_\ell > 32\%$				$\surd$

$36 < \Delta M < 53\,\mathrm{GeV}/c^2$						
BR_ℓ range	4J-H	2Jℓ-H	2Jτ-VH	2Jτ-H	$\ell\ell$-3	$\ell\tau$-3
$\mathrm{BR}_\ell < 10\%$	$\surd$	$\surd$	$\surd$			
$10\% < \mathrm{BR}_\ell < 17\%$	$\surd$	$\surd$	$\surd$	$\surd$		
$17\% < \mathrm{BR}_\ell < 22\%$		$\surd$	$\surd$	$\surd$		
$22\% < \mathrm{BR}_\ell < 27\%$		$\surd$	$\surd$	$\surd$	$\surd$	$\surd$
$27\% < \mathrm{BR}_\ell < 32\%$		$\surd$		$\surd$	$\surd$	$\surd$
$\mathrm{BR}_\ell > 32\%$					$\surd$	$\surd$

$25 < \Delta M < 36\,\mathrm{GeV}/c^2$					
BR_ℓ range	4J-H	2Jℓ-H	2Jτ-L	$\ell\ell$-3	$\ell\tau$-3
$\mathrm{BR}_\ell < 2\%$	$\surd$				
$2\% < \mathrm{BR}_\ell < 22\%$	$\surd$	$\surd$	$\surd$		
$22\% < \mathrm{BR}_\ell < 25\%$		$\surd$	$\surd$	$\surd$	
$25\% < \mathrm{BR}_\ell < 32\%$		$\surd$	$\surd$	$\surd$	$\surd$
$\mathrm{BR}_\ell > 32\%$				$\surd$	$\surd$

Table 3: *Combinations of neutralino selections as a function of ΔM for heavy sleptons.*

ΔM range (GeV/c^2)	Selections
$\Delta M < 15$ (higgsino region)	AJ-L
$15 < \Delta M < 20$ (higgsino region)	AJ-L.or.AJ-H
$20 < \Delta M < 40$ (higgsino region)	AJ-H
$\Delta M > 40$ (mixed region)	4Jγ.or.AJ-H

ratio into a single lepton flavour. The $\ell\ell$-3, $\ell\tau$-3, and $\tau\tau$-3 symbols refer to the Aℓ-3 selection in the $\ell\ell$, $\ell\tau$, and $\tau\tau$ topologies, respectively.

As expected, for larger leptonic branching ratios, the 4J selections contribute less to the overall efficiency and are eventually dropped from the combinations. In contrast, the Aℓ selections contribute more and are included for branching ratios in excess of 22% (depending on the mass difference). In the case considered here, where the three leptonic branching ratios are almost identical, the $\tau\tau$-3 selection is never used due to its larger background. The 2Jℓ selections have a low background and are used over most of the BR$_\ell$ range.

In the higgsino region, the optimal combination of neutralino AJ selections is determined as a function of ΔM. In the mixed region, the signal topologies vary rapidly, hence the combination of several selections is used all over that region.

The combinations used for neutralino production in the case of heavy sleptons are summarized in Table 3. The resulting signal efficiency for $\chi\chi'$ production in the higgsino region is shown in Fig. 2 as a function of ΔM, together with the expected background. This plot also includes results obtained for lower slepton masses since in the higgsino region the dominant topology consists of acoplanar jets even in that case. In the mixed region, a combination of the AJ-H and 4Jγ selections is used.

For large leptonic branching ratios, the combination of the AJ, Mℓ, and Aℓ-χ selections is used over most of the gaugino and mixed regions. Since, in these regions, the neutralino production processes and the leptonic and hadronic branching ratios change rapidly as a function of the parameters, such a combination provides a rather stable signal efficiency of typically 25% for slepton masses in excess of 80 GeV/c^2. For smaller slepton masses, invisible final states (due for instance to $\chi\chi'$ production with $\chi' \to \nu\tilde{\nu}$) become possible and give rise to a significant decrease in the neutralino sensitivity. The total background amounts to about 130 fb, out of which about 70 fb comes from WW production.

3.5 Systematic effects

Except in the case of dilepton final states where the WW background is taken into account, no background subtraction is performed in the extraction of the results. It is therefore sufficient to evaluate the systematic uncertainties related to the determination of the signal efficiency and to the WW $\to \ell\nu\ell\nu$ final state.

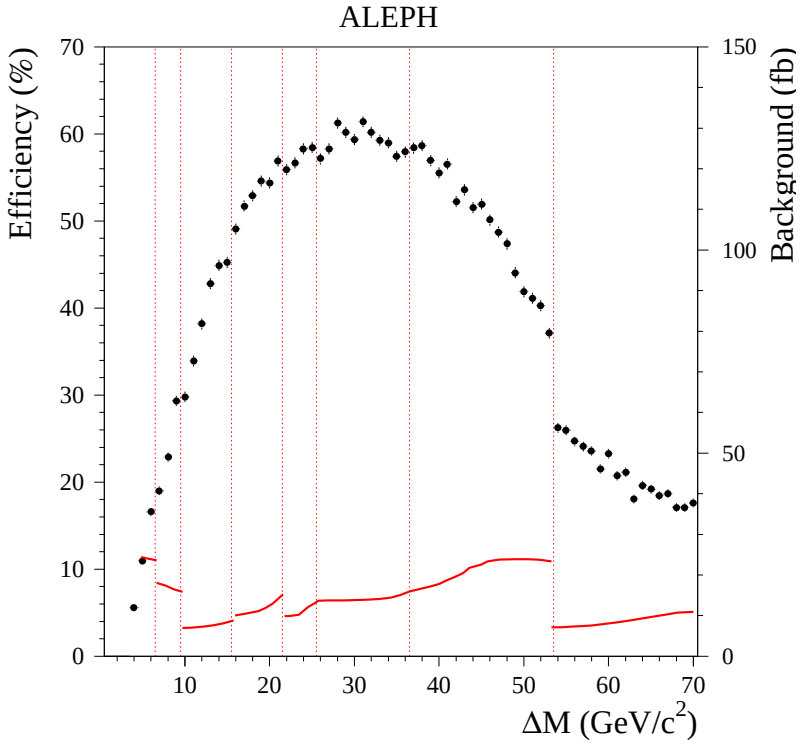

Figure 1: *Signal efficiency (dots) and total background (curves) for the chargino selection combinations as a function of ΔM for a 91 GeV/c^2 chargino and heavy sleptons.*

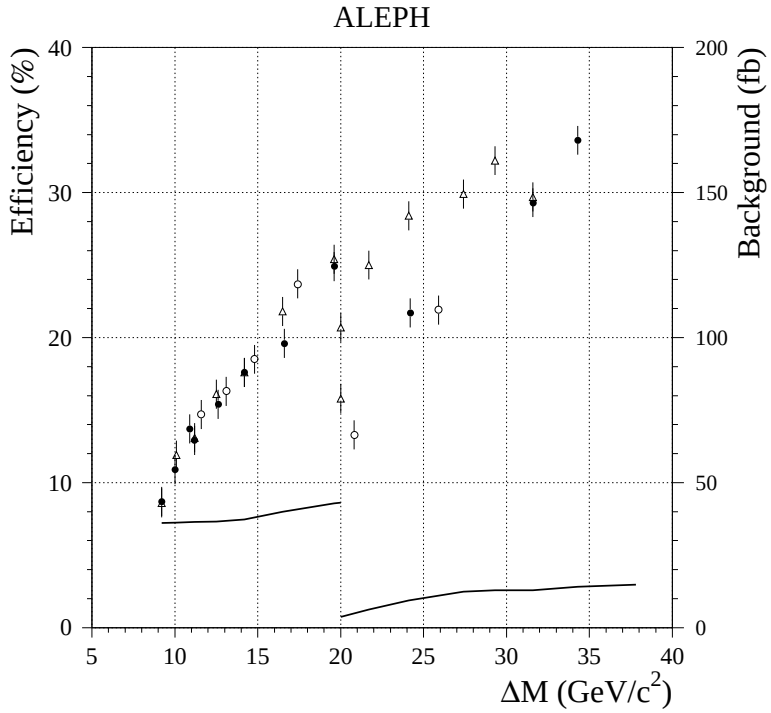

Figure 2: *The AJ selection efficiency for the $\chi\chi'$ channel in the higgsino region (symbols) and the expected background (lines) as a function of the mass difference between the two neutralinos. The different symbols refer to different values of the model parameters: m_0 = 200 GeV/c^2 and μ positive (open circles) or negative (triangles); m_0 = 75 GeV/c^2 and μ negative (full circles). In all cases, $\tan\beta = \sqrt{2}$.*

A fast simulation is used for neutralinos and for charginos away from the kinematic limit. A comparison of this fast simulation with the full simulation for a number of signal samples shows a very good overall agreement. When slight differences are seen, the fast simulation gives lower efficiencies. Conservatively, this effect is not corrected.

The various selections detailed above are very similar to those which were applied at lower energies. The main systematic errors, related to the simulation of the energy flow reconstruction and of lepton identification, were addressed in Ref. [4]. Their level is essentially unchanged for the 183 GeV data. These systematic uncertainties are included in the derivation of the results according to the method of Ref. [18]. They are also applied to the WW $\rightarrow \ell\nu\ell\nu$ background subtracted.

The beam-related background is expected to vary from year to year, as the centre-of-mass energy is increased. This background is not included in the event simulation and is taken into account separately. Its main effect is to contribute to E_{12}, the energy detected within 12° of the beam axis. The E_{12} distribution due to the beam-related background is determined using data collected at random beam crossings, and a contribution to E_{12}, generated according to that distribution, is added to the simulated signal events prior to the efficiency determination.

3.6 Selected events

The selections detailed above were applied to the 183 GeV data. The combinations of selections depend in general on the mass difference and on the leptonic branching ratios. The candidate events selected when heavy sleptons are assumed are presented first, those selected in the case of enhanced leptonic branching ratios next.

3.6.1 Heavy sleptons

Four events are selected by the combinations of selections listed in Tables 1 and 3. Due to the sliding cuts and to the transitions between combinations, each of them contributes to a limited range of ΔM, as shown in Table 4. Candidate 2 is selected in the data taken at $\sqrt{s} = 181.7\,\mathrm{GeV}$ and therefore does not contribute to the search for charginos with masses in excess of $91\,\mathrm{GeV}/c^2$. Candidate 3 is selected by both the chargino and neutralino searches. Candidate 4 contributes only to $\Delta M < 3.2\,\mathrm{GeV}/c^2$ where the selection efficiency is very small.

The fourth selected event is most likely due to the $\gamma\gamma \rightarrow$ hadrons process, to be compared to an expectation of 1.1 events. The expected background from other sources amounts to 4.4 events, with three candidate events observed.

Table 4: *Candidate events in the chargino and neutralino selections used in the case of heavy sleptons, together with their centre-of-mass energies and the ΔM ranges to which they contribute.*

candidate number	selection	$\sqrt{s}$ (GeV)	ΔM range (GeV/c^2)
1	2Jℓ-H	182.7	$\Delta M > 65.5$
2	2Jτ-VH 2Jτ-L 4J-H	181.7	$\Delta M > 31$
3	4J-H AJ-H	182.7	$19 < \Delta M < 53.5$ $\Delta M > 37.5$
4	2Jℓ-VL	182.7	$1.8 < \Delta M < 3.2$

3.6.2 Light sleptons

A total of 14 candidate events is selected in the data with the Aℓ chargino selections, while 18.7 events are expected from Standard Model processes. Each candidate affects a limited region of the (ΔM, BR$_\ell$) plane due to the sliding cuts.

Three events are selected in the data by the combination of neutralino analyses given in Section 3.4, whereas 7.2 are expected from Standard Model processes. Two of the observed events are selected by the Aℓ-χ analysis and are most likely due to WW production. They were also found by the slepton searches at 183 GeV reported in [2], and have to be compared with 4.1 events expected from WW$\rightarrow \ell\nu\ell\nu$. The third candidate event is selected by the AJ-H analysis (candidate 3 in Table 4).

4 Results and interpretation

The negative results of the searches for charginos and neutralinos described in the previous section can be translated into limits on the gaugino production cross sections and masses as well as into constraints on the MSSM parameter space. This is discussed in Section 4.1, first in the case of heavy sfermions and then in the case of light sfermions assuming scalar mass unification.

By combining the searches for charginos and neutralinos presented above with the searches for sleptons described in Ref. [2], the MSSM parameter space is further constrained, and a lower limit on the mass of the LSP is extracted as a function of $\tan\beta$ and m_0. The method and the results are presented in Section 4.2.

Exclusion regions in the MSSM parameter space can also be obtained from the Higgs boson searches described in Ref. [5]. More stringent constraints on the LSP mass can be derived by combining chargino, neutralino, slepton, and Higgs boson searches. This is discussed in Section 4.3.

Finally all results are interpreted in Section 4.4 within a more constrained model, minimal supergravity.

In all cases, the limits are given at the 95% confidence level. Whenever the kinematic limit is indicated, it corresponds to the highest energy point ($\sqrt{s}$ =183.8 GeV), at which 3% of the total integrated luminosity was collected.

4.1 Interpretation in the MSSM

Chargino searches can be used to derive an upper limit on the cross section for the production of chargino pairs. The result is shown in Fig. 3 for chargino masses close to the kinematic limit and for sfermion masses large enough for W exchange to dominate the decay. The discontinuities in the limit reflect mainly the changes in the number of candidates. Similarly, the upper limit on the cross section for $\chi\chi'$ production derived from neutralino searches is shown in Fig. 4 for the higgsino region ($\Delta M < 40\,\mathrm{GeV}/c^2$), where Z exchange dominates the decay. Apart from the assumption on the gaugino decay modes, these cross section limits can be considered as essentially model independent, although the selection efficiencies are slightly affected by the chargino and neutralino field content [4].

Within the MSSM, with the further constraint of gaugino mass unification at the GUT scale and assuming that all scalars are heavy enough to play a negligible rôle in the gaugino phenomenology, all masses, production cross sections, and decay branching ratios of charginos and neutralinos depend only on the parameters μ and M_2 for a given value of $\tan\beta$. Limits on the production of charginos and neutralinos can therefore be used to exclude regions in the (μ,M_2) plane. Such exclusions are shown in Fig. 5 for $\tan\beta = \sqrt{2}$ and in Fig. 6 for $\tan\beta = 35$. For small $\tan\beta$ and negative μ, neutralino searches allow chargino exclusions to be improved in most of the higgsino and mixed regions. In contrast, neutralino searches are ineffective in the gaugino region if sleptons are assumed to be heavy. The production via t channel does not contribute in that case, and the s channel contribution is suppressed because the higgsino component of the lightest neutralinos, responsible for their coupling to the Z, is small in the gaugino region.

These results translate into chargino mass limits in the gaugino and higgsino regions as shown in Fig. 7. Over most of the parameter space chargino searches exclude chargino masses to within $1\,\mathrm{GeV}/c^2$ of the kinematic limit. The deterioration of the limit for large M_2 is due to the fact that ΔM is small in the deep higgsino region, leading to a lower selection efficiency. For small $\tan\beta$ and negative μ, neutralino searches exclude chargino masses well beyond the kinematic limit for chargino-pair production. Similarly, Fig. 8 shows the lower limit on the sum of the masses of the two neutralinos produced with the largest cross section ($\chi\chi'$ for $M_2 > 110\,\mathrm{GeV}/c^2$ and mainly $\chi\chi''$ for $M_2 < 110\,\mathrm{GeV}/c^2$) as a function of M_2. The limit is within $3\,\mathrm{GeV}/c^2$ of the kinematic limit over most of the higgsino region. The irregularities in the mixed region reflect the rapid changes in the production processes ($\chi\chi', \chi\chi'', \chi'\chi''$) and decay branching ratios. The limit deteriorates at small M_2 due to the larger four-fermion background selected by the analyses aimed at $\Delta M > 40\,\mathrm{GeV}/c^2$. Figure 8 demonstrates that the different behaviour of the indirect limit on the chargino mass from

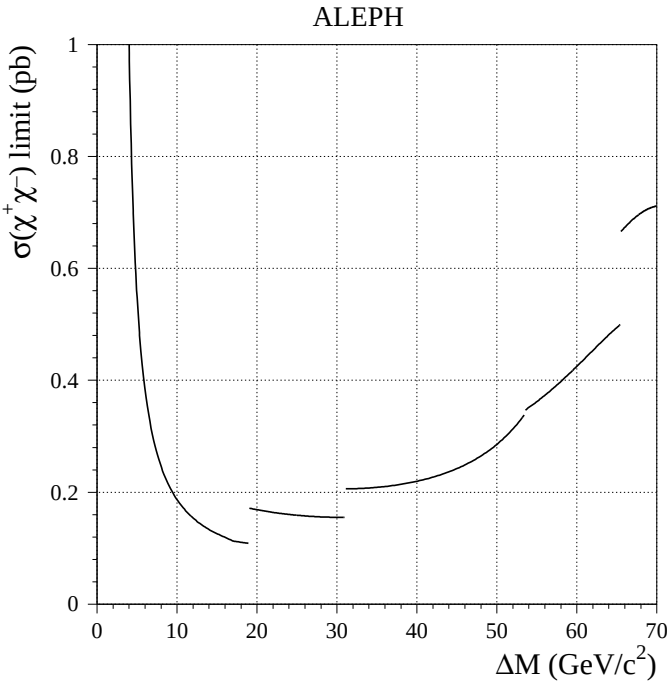

Figure 3: *The 95% C.L. upper limit on the chargino production cross section for charginos of mass 91 GeV/c^2 and for heavy sleptons, as a function of the mass difference between the chargino and the lightest neutralino.*

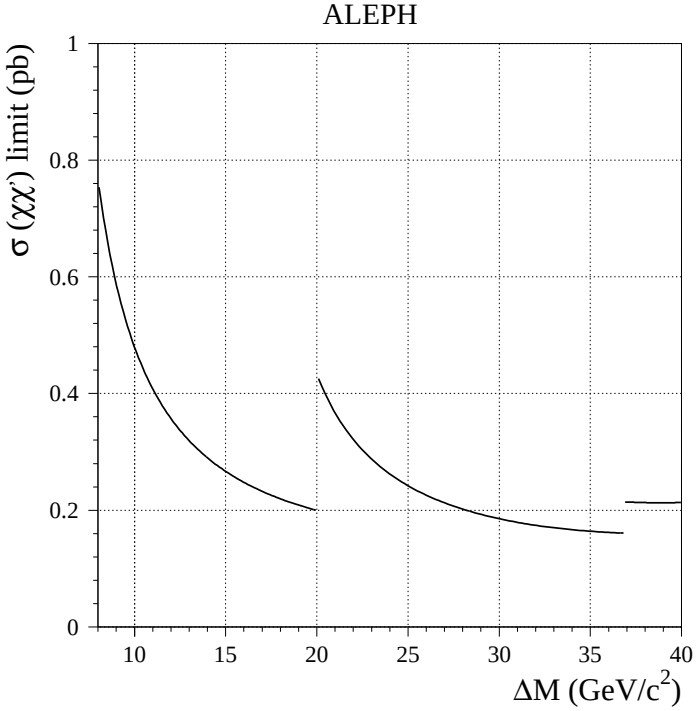

Figure 4: *The 95% C.L. upper limit on the $\chi\chi'$ production cross section in the higgsino region close to the kinematic limit, as a function of the mass difference between the two neutralinos.*

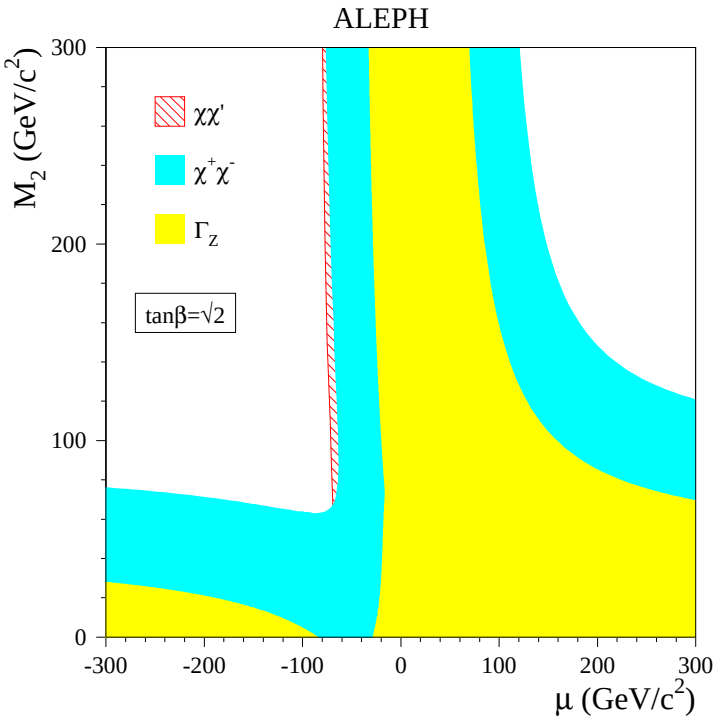

Figure 5: *Regions in the (μ,M_2) plane excluded at 95% C.L. by chargino (dark shading) and neutralino (hatched) searches for $\tan\beta = \sqrt{2}$ and $m_0 = 200$ GeV/c^2.*

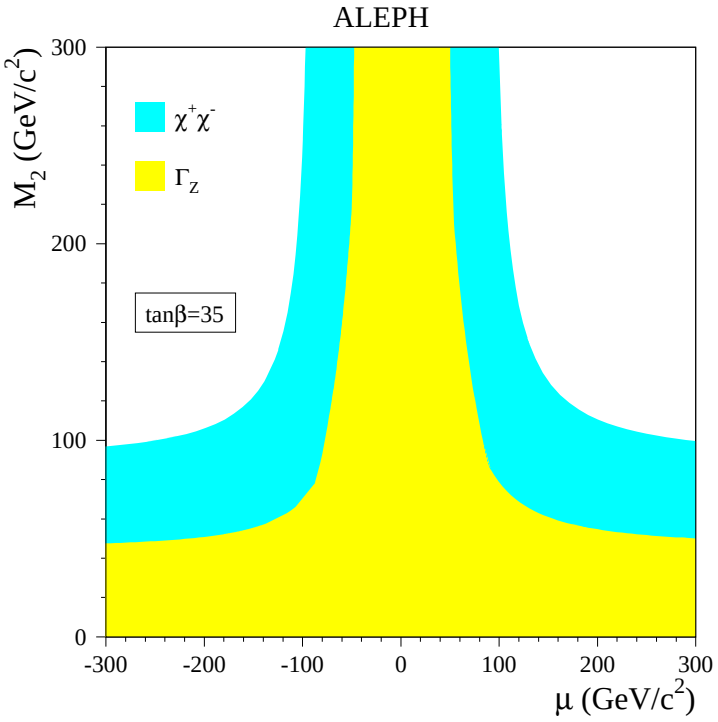

Figure 6: *Region in the (μ,M_2) plane excluded at 95% C.L. by chargino searches (dark shading) for $\tan\beta = 35$ and $m_0 = 200$ GeV/c^2.*

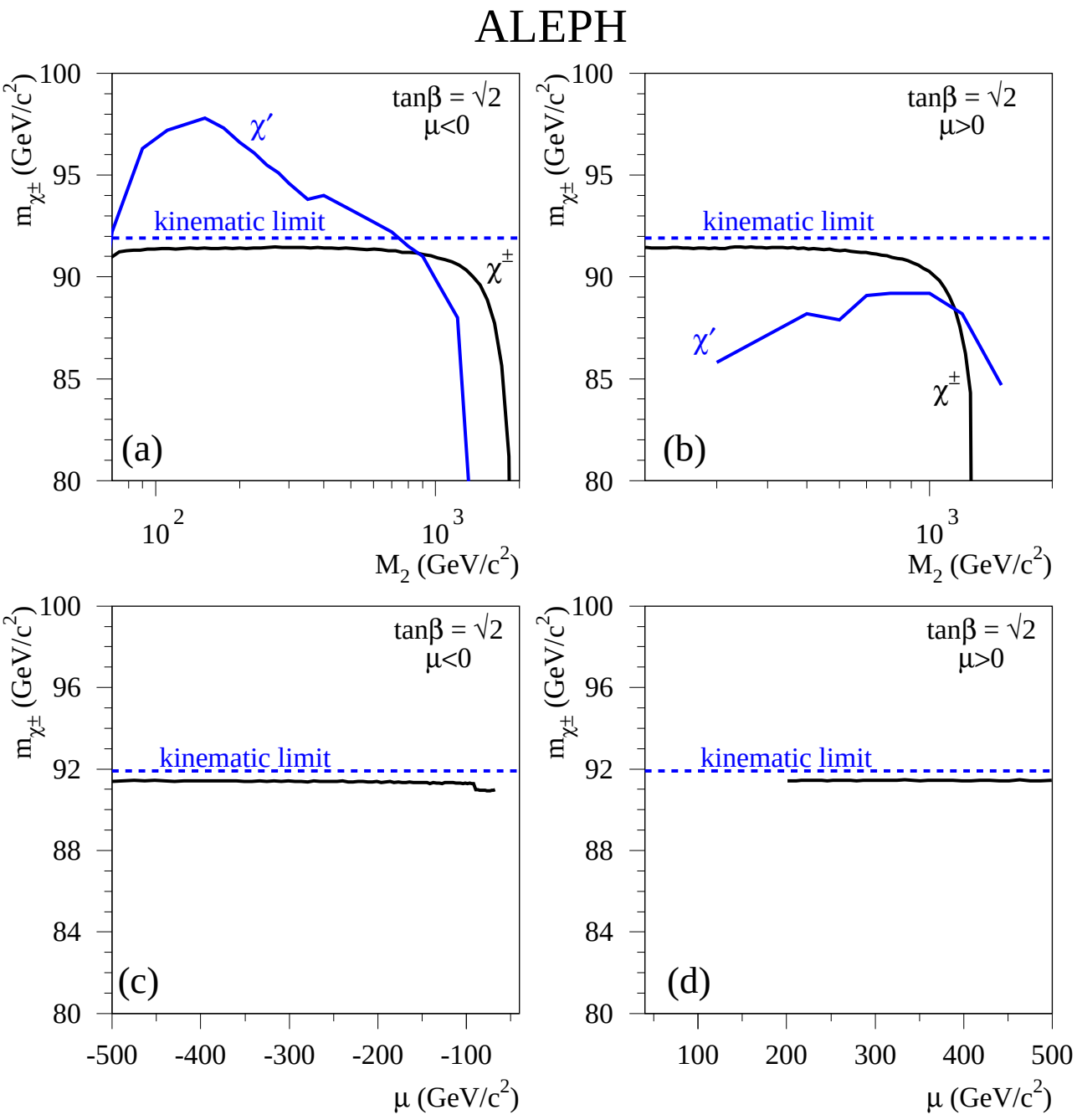

Figure 7: *The 95% C.L. lower limits on the chargino mass obtained for $tan\,\beta = \sqrt{2}$ and $m_0 = 200$ GeV/c^2 in the higgsino region (a,b) and in the gaugino region (c,d). In (a) and (b), the results of neutralino searches are translated into chargino mass limits.*

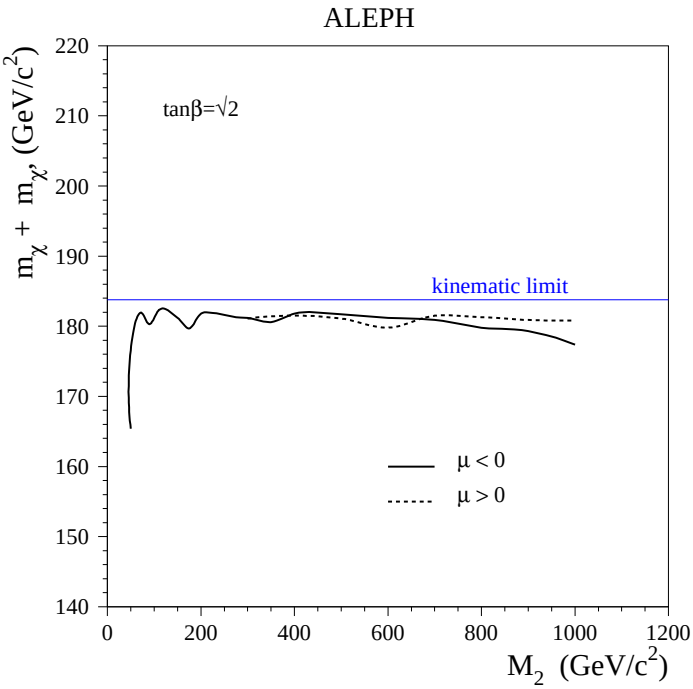

Figure 8: *The 95% C.L. lower limit on the sum of the masses of the two neutralinos produced with the largest cross-section ($\chi\chi'$ for $M_2 > 110$ GeV/c^2 and mainly $\chi\chi''$ for $M_2 < 110$ GeV/c^2) as a function of M_2 for $m_0 = 200$ GeV/c^2 and $\tan\beta = \sqrt{2}$. The full curve is for negative μ, the dashed curve is for positive μ.*

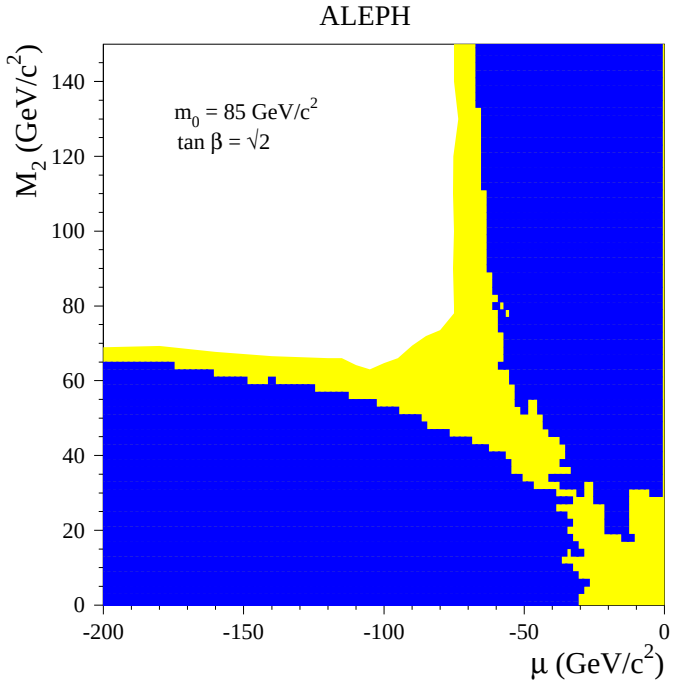

Figure 9: *Regions in the (μ,M_2) plane excluded at 95% C.L. by chargino (black region) and neutralino (grey region) searches for $\tan\beta = \sqrt{2}$ and $m_0 = 85$ GeV/c^2. The discontinuities in the chargino contour reflect the step size used in the scan of the parameter space.*

neutralino searches for μ positive and negative, shown in Fig. 7, is due to features of the mapping of the physical masses into the MSSM parameter space rather than to a difference in the mass reach of the neutralino search.

The case of small scalar masses is studied under the additional hypothesis that the soft supersymmetry breaking masses of all sleptons and squarks unify, at the GUT scale, to a common value m_0. In this way the chargino and neutralino production cross sections and their decay branching ratios are correlated. Because of too large a background from WW production, chargino searches become less efficient when sleptons are light (small m_0). As a consequence, a new unexcluded region develops in the (μ, M_2) plane, as shown in Fig. 9 for $m_0 = 85\,\mathrm{GeV}/c^2$. In this range of m_0, however, the neutralino sensitivity extends over the full mixed region and up to the deep gaugino region, thus filling this unexcluded domain. The neutralino sensitivity reaches a maximum for $m_0 \sim 80\,\mathrm{GeV}/c^2$. For larger m_0 values the cross section decreases because of the decreasing contribution of the t channel, while for smaller m_0 values the detection efficiency decreases because of the increasing invisible branching ratios (*e.g.*, for $\chi' \to \nu\tilde{\nu}$).

The lower limit on the chargino mass obtained in the gaugino region for m_0=$85\,\mathrm{GeV}/c^2$ is shown in Fig. 10. It can be seen that the limit from direct chargino searches is much weaker than in the case of large scalar masses. When approaching the mixed region, indirect limits from neutralino searches reach the kinematic limit for chargino production.

The above results are obtained with the assumption of no mixing in the stau sector. The impact of mixing was studied in detail in Ref. [4] and found to be small. The chargino and neutralino phenomenologies are also rather insensitive to the unification hypothesis for squark masses.

4.2 Limit on the LSP

In the case of large scalar masses, chargino searches alone allow a lower limit on the mass of the lightest neutralino to be set indirectly for any given $\tan\beta$. This limit is improved for low $\tan\beta$ values when constraints inferred from the total and invisible Z width measurements [19] and from direct searches for neutralinos [20] at LEP1 are taken into account. The result is shown in Fig. 11 for $m_0 = 500\,\mathrm{GeV}/c^2$. It can be seen that neutralinos lighter than $29\,\mathrm{GeV}/c^2$ are excluded in that case for any value of $\tan\beta$. This limit is robust for larger m_0 values.

For low enough m_0 values, chargino searches alone are no longer sufficient to set a lower limit on the mass of the lightest neutralino, for the reasons explained above. However, neutralino production is enhanced, which allows neutralino searches to extend the domain of sensitivity in the regions where the invisible decays such as $\chi' \to \nu\tilde{\nu}$ are not the dominant ones. Furthermore, lower m_0 values correspond to smaller slepton masses. Slepton searches [2] can therefore be used to restrict the allowed configurations in the MSSM parameter space. The expected lower limit on the LSP mass turns out to be larger if only the constraints from selectron production, which benefits from a larger cross section than that of the other slepton species with a similar background level, are used.

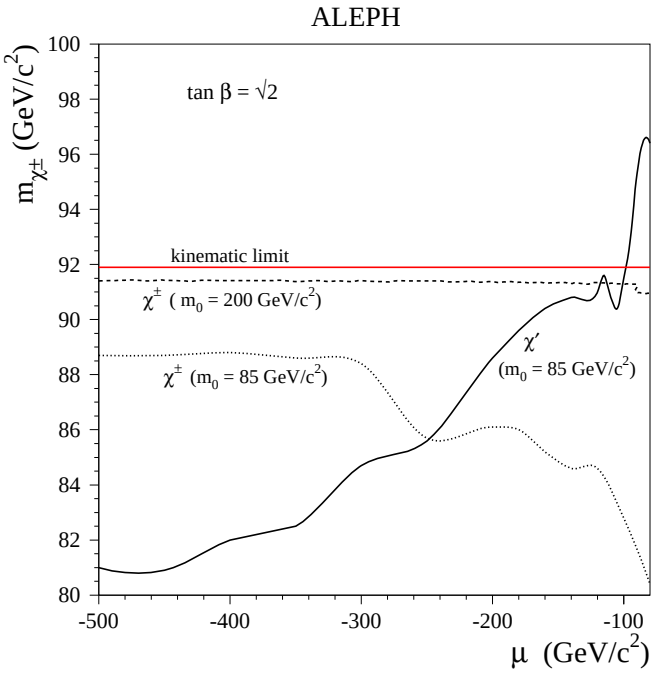

Figure 10: *The 95% C.L. lower limit on the chargino mass for tan $\beta = \sqrt{2}$ in the gaugino region. The dashed curve is the limit obtained from chargino searches for $m_0 = 200$ GeV/c^2. The dotted curve is the limit obtained from chargino searches for $m_0 = 85$ GeV/c^2. The black curve is the limit obtained from neutralino searches for $m_0 = 85$ GeV/c^2.*

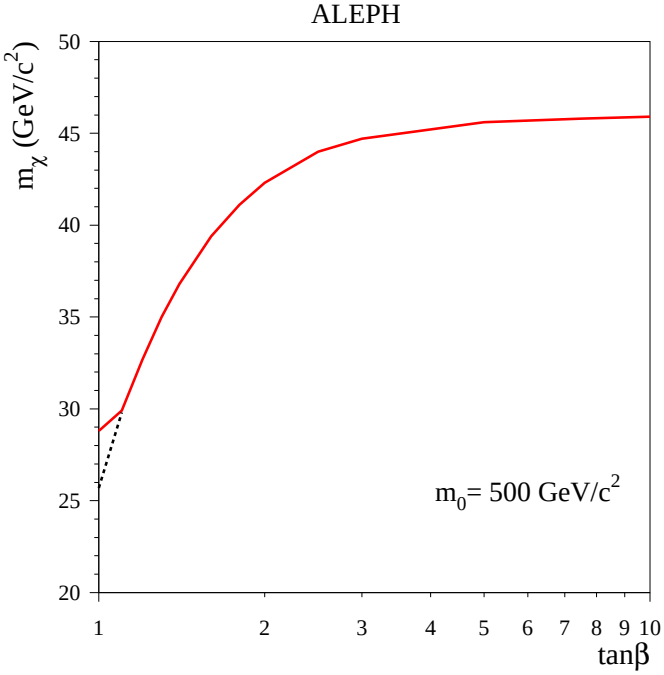

Figure 11: *Lower limit on the mass of the lightest neutralino as a function of tan β for $m_0 = 500$ GeV/c^2. Higher m_0 values give similar limits. The limit obtained without the LEP1 constraints is shown as a dashed line.*

An example of the interplay of these various constraints is shown in Fig. 12 for $\tan\beta = \sqrt{2}$ and $m_0 = 75\,\mathrm{GeV}/c^2$. Here the focus is set on the mixed region, corresponding to moderate values of M_2 ($M_2 < 150\,\mathrm{GeV}/c^2$) and to moderate and negative values of μ ($|\mu| < 200\,\mathrm{GeV}/c^2$). The motivation for this choice is that previous mass limits for the lightest neutralino [21, 22] were obtained in that region, which is moreover the scene of rapid variations in production cross sections and decay patterns. The unexcluded region kinematically accessible to chargino searches largely corresponds to the occurrence of two-body leptonic decays. The exclusion by selectron searches would be almost equivalent to a lower limit on M_2 if cascade decays such as $\widetilde{\mathrm{e}}_R \to \mathrm{e}\chi'$ with $\chi' \to \chi\gamma$, for which a null efficiency is conservatively assumed, were not present. In contrast to the case of chargino and slepton searches, for which it is practical and sufficient to produce selection efficiency maps for the main decay channels ($\chi^\pm \to \chi \mathrm{q}\,\overline{\mathrm{q}}'$, $\chi^\pm \to \chi\ell\nu$, $\chi^\pm \to \ell\tilde{\nu}$, $\widetilde{\mathrm{e}}_R \to \mathrm{e}\chi$), it is necessary for the neutralino searches to perform complete simulations of all production and decay processes because of the large and rapid variations which take place in the mixed region. The combined exclusion is shown in Fig. 13. Altogether, a lower limit on the mass of the LSP of $35\,\mathrm{GeV}/c^2$ is obtained in this example.

Similar studies for several values of m_0 and $\tan\beta$ lead to the conclusion that the limit on the LSP mass is $28\,\mathrm{GeV}/c^2$ in the mixed region, for any $\tan\beta$ and any m_0. This limit is reached in the so-called *corridor* [4, 21] where the chargino and sneutrino are mass degenerate. The lepton from the $\chi^\pm \to \ell\tilde{\nu}$ decay is practically invisible, the heavier neutralinos kinematically within reach decay invisibly, and at the same time the selectron mass is at its experimental limit. Extending these investigations into the gaugino region (moderate M_2 and larger $|\mu|$), the χ mass lower limit obtained in the mixed region is found to be robust for $\tan\beta < 6$. For larger values of $\tan\beta$, the limit progressively degrades but remains above $27\,\mathrm{GeV}/c^2$, a value reached asymptotically for very large $\tan\beta$, in the deep gaugino region and for $m_0 = 70\,\mathrm{GeV}/c^2$.

The evolution of the LSP limit with $\tan\beta$ and m_0 is illustrated in Fig. 14. The limit as a function of $\tan\beta$ is shown in Fig. 14a for $m_0 = 75\,\mathrm{GeV}/c^2$ whereas the limit as a function of m_0 is shown in Fig. 14b for $\tan\beta = \sqrt{2}$. For $m_0 = 75\,\mathrm{GeV}/c^2$ it can be seen that neutralino searches at LEP2 are needed in order to exclude a massless LSP for $\tan\beta = 1$. Increasing slepton masses are responsible for the degradation of the limit with increasing $\tan\beta$ up to 1.8. At that point, the limit improves again because the chargino contribution takes over. This improvement is due to the fact that the mass difference between the chargino and the LSP decreases with increasing $\tan\beta$; therefore, a given chargino mass limit excludes larger χ masses for larger $\tan\beta$. For $\tan\beta = \sqrt{2}$, the limit first deteriorates with m_0 because the slepton mass increases. For larger m_0 the limit stabilizes because of the enhanced chargino and neutralino sensitivities: the chargino production cross section increases and the invisible $\chi' \to \nu\tilde{\nu}$ decays become kinematically closed.

Extending the gaugino mass unification condition to gluinos, limits obtained at $\mathrm{p\overline{p}}$ colliders could also be considered in the present context. The published results are however difficult to use in a detailed scan of the MSSM parameter space such as the one performed here because they are given for specific choices of μ and $\tan\beta$. It is nevertheless interesting to see whether some improvement can be expected in the simplest case of large m_0 and

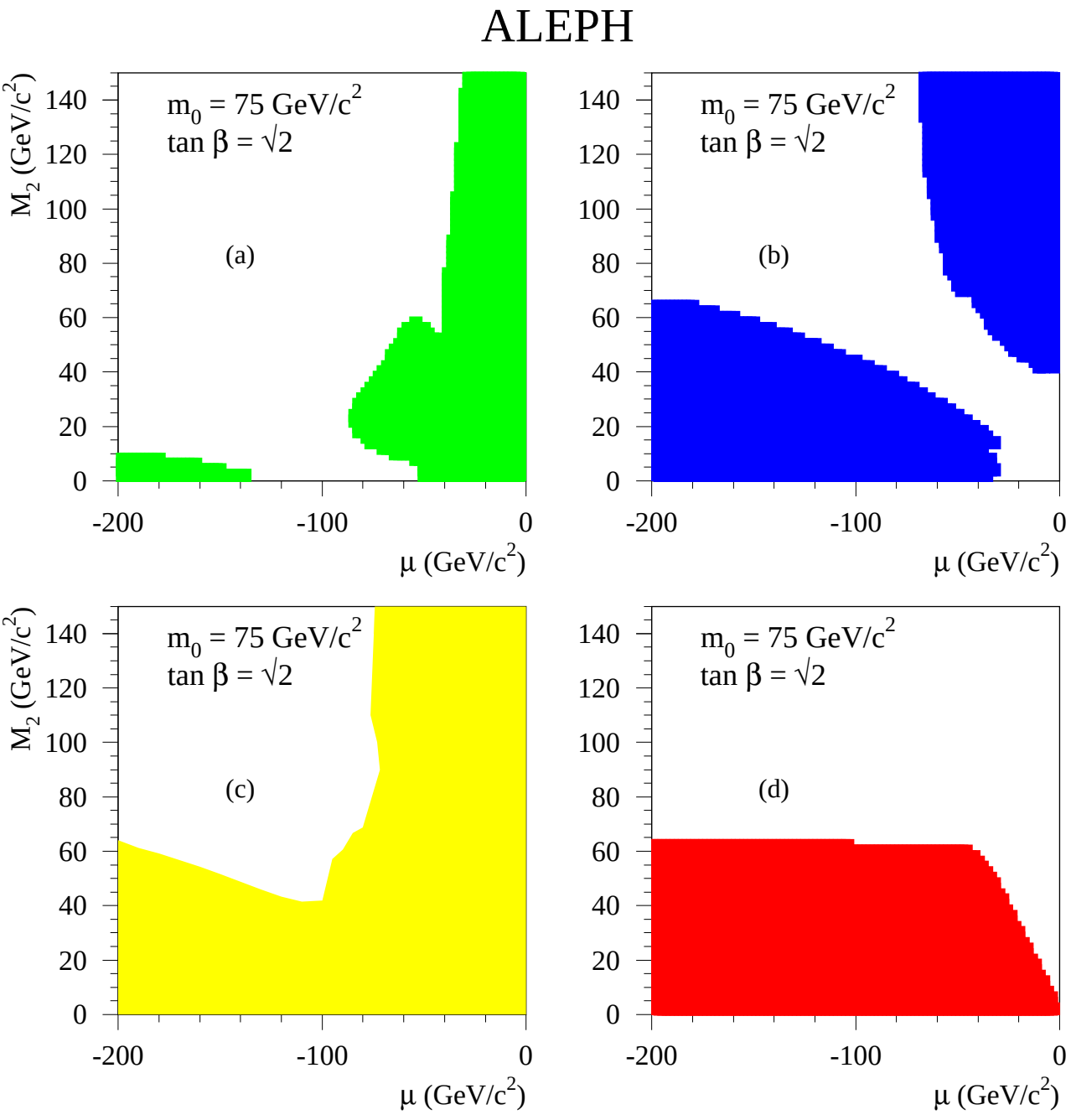

Figure 12: *Regions in the (μ,M_2) plane excluded by searches at LEP1 (a), by chargino searches at 183 GeV (b), by neutralino searches at 183 GeV (c) and by selectron searches at LEP2 (d), for $\tan\beta = \sqrt{2}$ and $m_0 = 75$ GeV/c^2.*

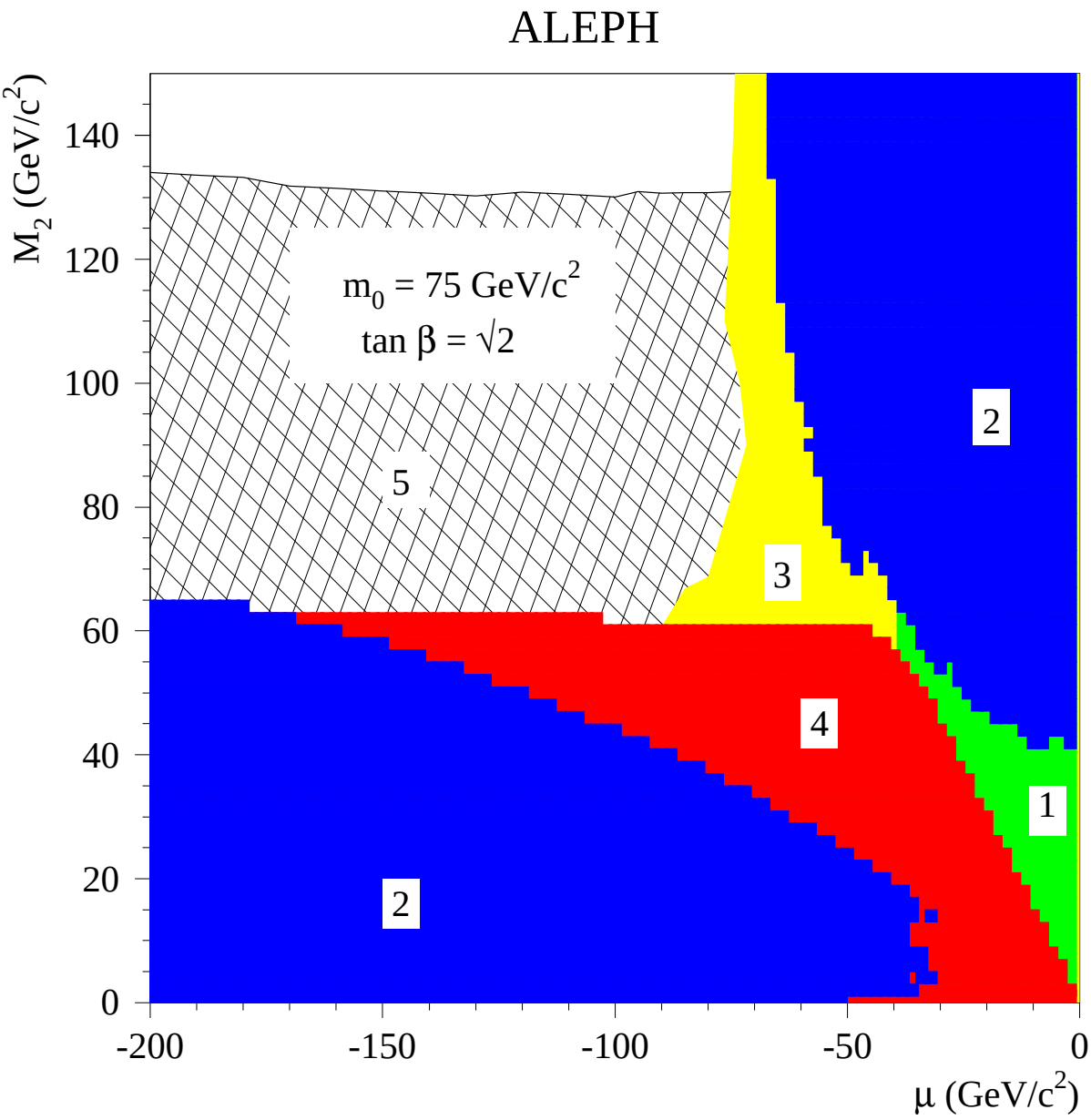

Figure 13: *Regions in the (μ,M_2) plane excluded by the combination of LEP1 constraints (1), and of chargino (2), neutralino (3), and slepton (4) searches at LEP2 for $\tan\beta = \sqrt{2}$ and $m_0 = 75$ GeV/c^2. The region excluded by the Higgs boson searches at LEP2 is also shown (5).*

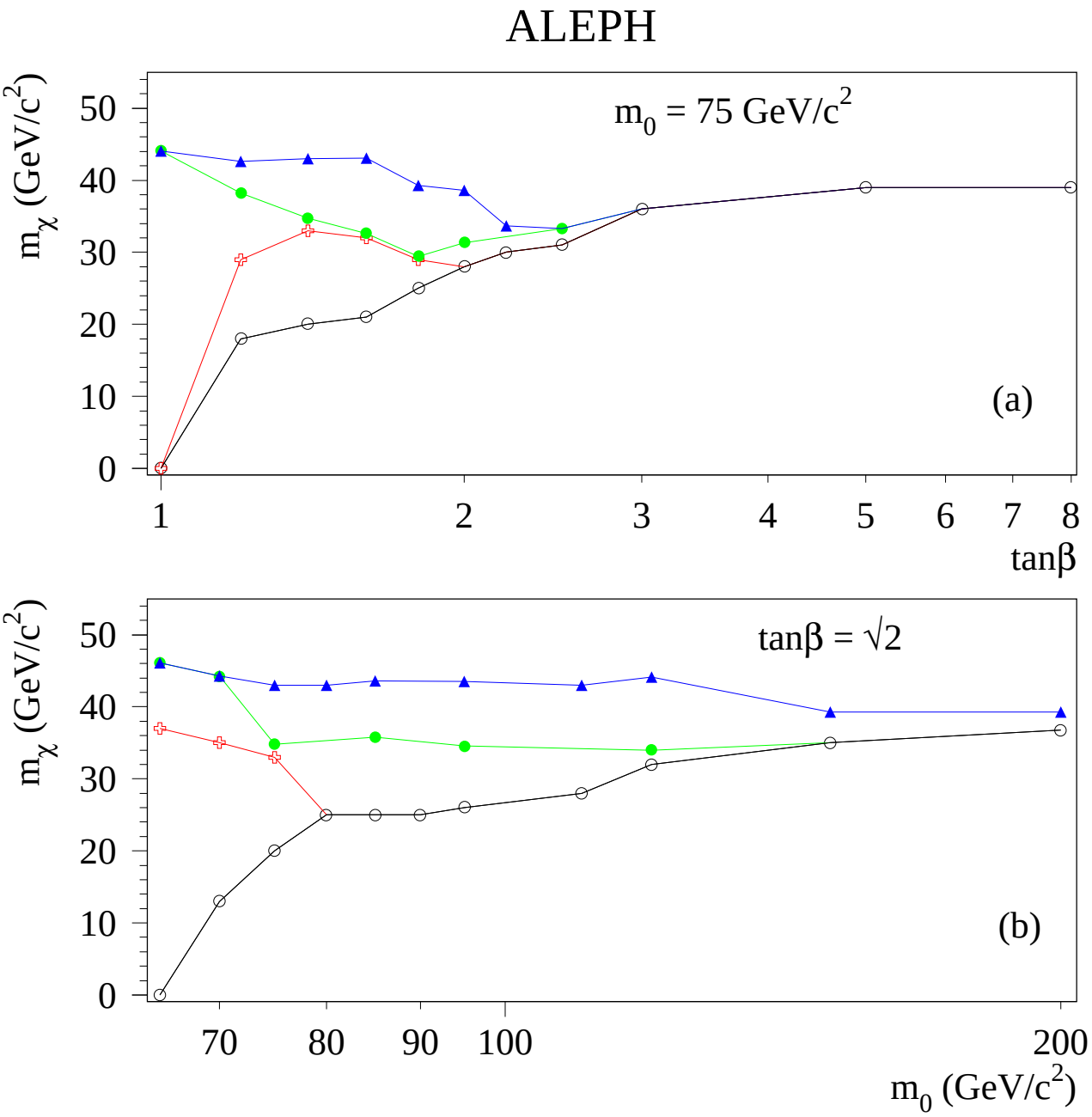

Figure 14: *Limit on the mass of the lightest neutralino as a function of tan β for $m_0 = 75$ GeV/c^2 (a) and as a function of m_0 for tan $\beta = \sqrt{2}$ (b). The open circles represent the results obtained using the LEP1 constraints and chargino searches only, the crosses those obtained when the slepton searches are included, and the dots those obtained when the neutralino searches are included in addition. The results obtained with the Higgs boson searches also taken into account are represented by triangles.*

low $\tan\beta$. The best published gluino mass limit is $173\,\mathrm{GeV}/c^2$ [23], obtained for $\tan\beta = 2$ and $\mu = -200\,\mathrm{GeV}/c^2$. For μ values smaller than $-100\,\mathrm{GeV}/c^2$ or larger than $200\,\mathrm{GeV}/c^2$ and for several values of $\tan\beta$, the limit remains within $10\,\mathrm{GeV}/c^2$ of that value. It can be turned into a lower limit of $47\,\mathrm{GeV}/c^2$ on M_2 (for $\alpha_s(m_\mathrm{Z}) = 0.12$) in that same μ range. Even if this result could be extended into the mixed region, where the LSP mass limit from the present analysis is set for large m_0, no improvement would be obtained, although the sensitivity would be similar for $\tan\beta = 1$.

4.3 Interpretation in the MSSM including Higgs boson searches

For low values of m_0 and $\tan\beta$, constraints on the parameter space of the MSSM can also be inferred from searches in the Higgs sector. At tree level, the mass m_h of the lighter CP-even Higgs boson depends only on the mass m_A of the CP-odd Higgs boson and on $\tan\beta$. The value of m_h ranges from zero, for $m_\mathrm{A} = 0$, to a maximum value of $m_\mathrm{Z}|\cos 2\beta|$ for very large values of m_A. Therefore, a lower limit on m_h trivially translates into a lower limit on $\tan\beta$.

When the radiative corrections due to the large top quark mass are taken into account, the square of this upper bound is increased, at the one-loop level, by [24]

$$\frac{3g^2}{8\pi^2}\frac{m_\mathrm{t}^4}{{m_\mathrm{W}}^2}\log\frac{m_{\tilde{\mathrm{t}}}^2}{m_\mathrm{t}^2}.$$

Here, the two stops are assumed to be mass-degenerate and $m_{\tilde{\mathrm{t}}}$ is the stop mass. For $m_{\tilde{\mathrm{t}}}$ not much larger than m_t, this correction may be sufficiently small to still allow a lower limit on $\tan\beta$ to be obtained. Alternatively, for a given (low) value of $\tan\beta$, a minimum value for $m_{\tilde{\mathrm{t}}}$ can be inferred from the lower limit on m_h. In supergravity inspired models with universal soft SUSY-breaking sfermion m_0 and gaugino $m_{1/2}$ masses at the grand unification scale, the stop mass at the weak scale receives contributions from both of those, which allows the lower limit on $m_{\tilde{\mathrm{t}}}$ to be translated into a lower limit on $m_{1/2}$, once a (low) value of m_0 is chosen.

This simple picture needs to be refined when stop mixing is taken into account. The main effect of stop mixing is to increase the size of the radiative corrections, and therefore to further raise the upper bound on the Higgs boson mass. However, at the same time, one of the stops becomes lighter, possibly very light, and results obtained in the stop sector become constraining. It is this interplay between Higgs boson and stop mass lower limits which still allows $m_{1/2}$ to be constrained for low values of $\tan\beta$ and m_0. For small mixing, the limits on m_h provide the most effective constraint, while for large mixing, limits on $m_{\tilde{\mathrm{t}}}$ play the major rôle.

To derive the results presented below, the radiative corrections in the Higgs sector from Ref. [25] have been used. The left and right squark masses are calculated from m_0 and $m_{1/2}$ using the renormalization group equations as given in Ref. [26], but without the effect of the top Yukawa coupling. (Since the effect of this coupling is to reduce the stop masses, the results presented here can be considered conservative.) Universality of squark SUSY-breaking masses at the GUT scale is assumed, but the Higgs sector is treated independently

and radiative breaking of the electroweak symmetry is not enforced, thus leaving $m_{\rm A}$ and μ as free parameters. Stop mixing is controlled by μ and by the trilinear coupling $A_{\rm t}$ through the combination $\tilde{A}_{\rm t} = A_{\rm t} - \mu \cot\beta$.

To decide whether a given set of $\{\tan\beta, m_{1/2}, m_0, \mu, A_{\rm t}, m_{\rm A}\}$ values, from which all relevant physical quantities can be calculated, is experimentally excluded or not, a variety of ALEPH results is used as explained in detail in Ref. [5]. The main constraints come from the neutral Higgs boson searches at LEP2 [5, 27]. In addition, the results pertaining to the chargino and neutralino sectors reported in the previous sections are used, as well as those from searches at LEP2 for invisible [28] and charged [29] Higgs bosons, for scalar leptons [2] and for scalar quarks [3], together with various LEP1 results [30].

In practice, an excluded domain in the $(m_{1/2}, \mu)$ plane is determined for a given choice of $\tan\beta$ and m_0. For each $\{\tan\beta, m_0, m_{1/2}, \mu\}$ set, a scan of the range of physically acceptable $A_{\rm t}$ values, *i.e.*, leading to stop masses larger than the χ mass, is performed and the set is rejected if it is excluded throughout the explored $A_{\rm t}$ range.

The result obtained by fixing $m_{\rm A} = 1\,\mathrm{TeV}/c^2$ is shown as a dashed curve in Fig. 15 for $\tan\beta = \sqrt{2}$ and $m_0 = 75\,\mathrm{GeV}/c^2$. The M_2 limit ($M_2 = 0.82\,m_{1/2}$) is almost independent of μ. The reason is that the main influence of μ comes through the stop mixing, *i.e.*, via the $\tilde{A}_{\rm t}$ combination, so that a change in μ can essentially be compensated by a change in $A_{\rm t}$. For most of the μ range considered, the M_2 limit at 130 to $150\,\mathrm{GeV}/c^2$ is well above the limit inferred from direct searches for supersymmetric particles. However, there are also μ regions in which no improvement is achieved. This is due to the occurrence of configurations where the stop and χ are almost mass degenerate. The experimental searches for stops require a minimal mass difference between the stop and the LSP, and are inefficient, *e.g.*, for long-lived stops. When the requirement $m_{\tilde{\rm t}} > m_\chi + 2\,\mathrm{GeV}/c^2$ is imposed, so that the $\tilde{\rm t} \to \chi{\rm c}$ decay is allowed, these gaps are greatly reduced but do not disappear completely, as shown by the dotted curve in Fig. 15. This constraint is imposed in the rest of this subsection.

The choice $m_{\rm A} = 1\,\mathrm{TeV}/c^2$ may seem conservative since it leads to large values of $m_{\rm h}$, close to its upper bound. Fine tuned combinations of parameters have however been identified [5] with an unexcluded light Higgs boson h, and such that $m_{\rm A}$ is much smaller than $1\,\mathrm{TeV}/c^2$. This renders necessary a further scan in $m_{\rm A}$ for each $\{\tan\beta, m_{1/2}, m_0, \mu, A_{\rm t}\}$ set considered. The scan procedure is identical to that described in Ref. [5]. The result for $\tan\beta = \sqrt{2}$ and $m_0 = 75\,\mathrm{GeV}/c^2$ is shown as a continuous curve in Fig. 15. The improvement in the exclusion range remains appreciable, in particular in the mixed region as shown in Fig. 13. The degradation with respect to the result obtained for fixed $m_{\rm A} = 1\,\mathrm{TeV}/c^2$ is due to the occurrence of pathological sets of parameters such as those discussed in Ref. [5]. The improvement over the limit derived from chargino searches vanishes for large values of $|\mu|$ ($\mu < -1.2\,\mathrm{TeV}/c^2$ or $\mu > 1.4\,\mathrm{TeV}/c^2$). Nevertheless, the χ mass lower limit for $\tan\beta = \sqrt{2}$ and $m_0 = 75\,\mathrm{GeV}/c^2$ improves from 35 to $43\,\mathrm{GeV}/c^2$.

The same procedure was applied for several values of $\tan\beta$ and m_0. Examples of results are shown in Fig. 14. The improvement in the χ mass limit is quite substantial, but as anticipated, it is limited to the lower $\tan\beta$ and m_0 values. The $\tan\beta$ and m_0 independent lower limit of $27\,\mathrm{GeV}/c^2$, obtained for large $\tan\beta$ as explained in the previous section, is therefore not affected.

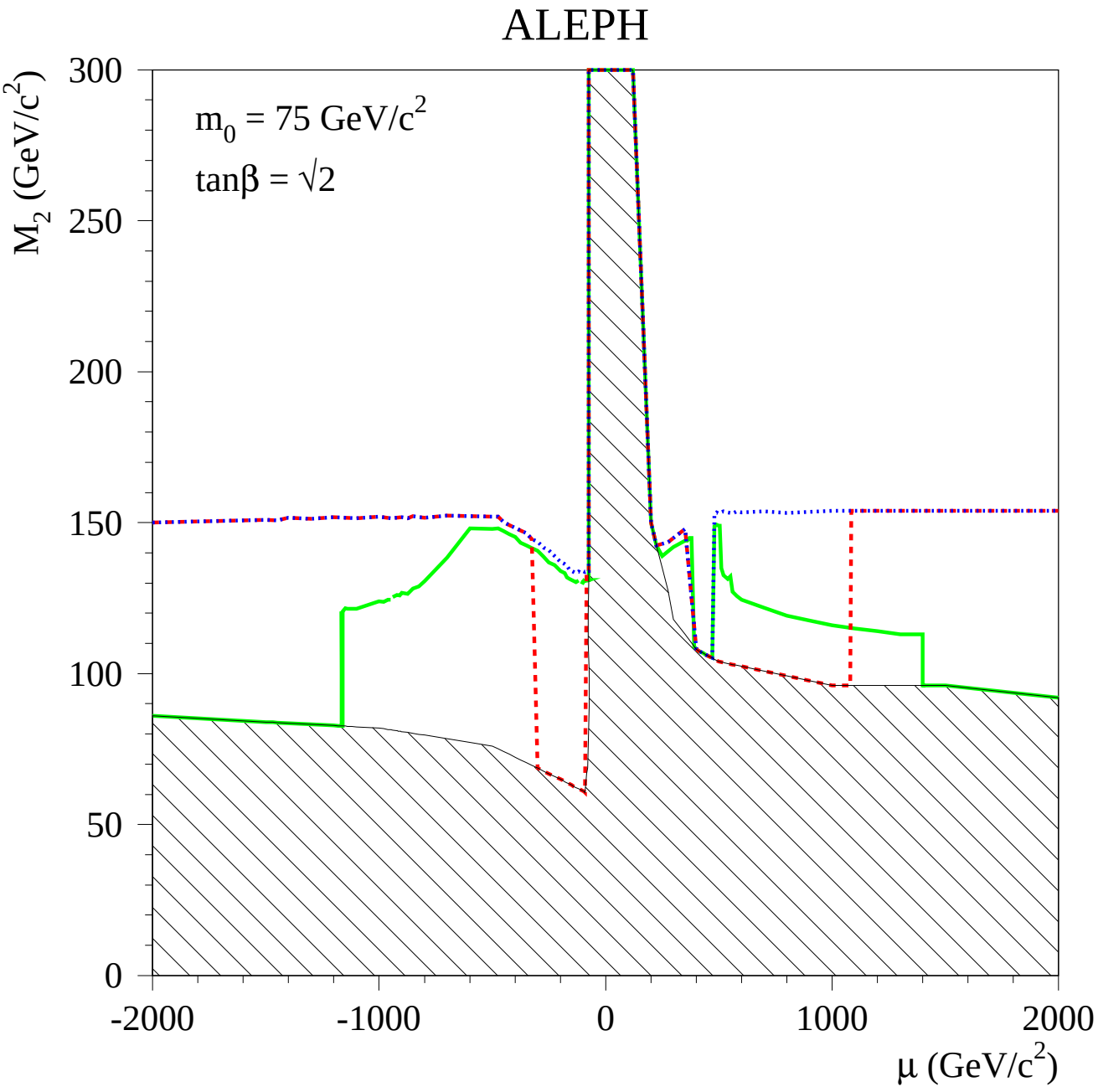

Figure 15: (M_2, μ) *plane for* $\tan\beta = \sqrt{2}$ *and* $m_0 = 75$ *GeV*/c^2. *Limits from SUSY searches (hatched) and from Higgs boson searches: for* $m_{\mathrm{A}} = 1$ *TeV*/c^2 *(dashed); for* $m_{\mathrm{A}} = 1$ *TeV*/c^2 *and* $m_{\tilde{\mathrm{t}}} > m_{\chi} + 2$ *GeV*/c^2 *(dotted); for any* m_{A} *and* $m_{\tilde{\mathrm{t}}} > m_{\chi} + 2$ *GeV*/c^2 *(full). Unlike in the previous plots, here the* μ *axis expands to* ± 2 *TeV*/c^2.

4.4 Interpretation in minimal supergravity

The results presented so far were derived in the context of a semi-constrained MSSM, with six relevant parameters: $\tan\beta$, $m_{1/2}$, m_0, μ, A_t and m_A. The number of parameters can be further reduced within the framework of minimal supergravity [6]. The hypothesis of unification at the GUT scale of all soft supersymmetry breaking scalar masses, *i.e.*, now including also those pertaining to the Higgs sector, removes m_A from the list of independent parameters. The constraint of a correct electroweak symmetry breaking, dynamically triggered by the radiative corrections due to the large top Yukawa coupling, allows μ to be calculated from the other parameters up to a sign ambiguity. The trilinear couplings for all scalars are also assumed to unify to a common value A_0 at the GUT scale.

The remaining parameters are therefore $m_{1/2}$, m_0, A_0, $\tan\beta$ and the sign of μ. The physically acceptable set of values for these parameters is restricted by the requirements that the top Yukawa coupling should not develop a Landau pole up to the GUT scale, and that none of the scalar particles should be tachyonic. The ISAJET package [31], with the top quark mass set to $175\,\mathrm{GeV}/c^2$, was used to obtain the results presented below.

Exclusion domains in the $(m_0, m_{1/2})$ plane are shown in Figs. 16 and 17 for $\tan\beta = 2$, 3, 10 and 35, for $\mu < 0$ and $\mu > 0$, and for $A_0 = 0$. In all cases, the theoretical constraints restrict the allowed sets of $\{m_0, m_{1/2}\}$ values. Large regions are excluded by the Higgs boson searches, in particular for low $\tan\beta$ and negative μ. Slepton searches contribute most effectively for low m_0, while the constraints from the Z width measurement at LEP1 and from chargino searches at LEP2 forbid low $m_{1/2}$ values.

The interplay between chargino, Higgs boson and slepton searches reduces the impact of the small ΔM *corridor* visible in the chargino exclusion area as a vertical strip. In Fig. 18, a zoom on the corridor region is shown for $\tan\beta = 4$ and $\mu < 0$. In this specific case, the Z width measurement and chargino direct searches set a lower limit on $m_{1/2}$ of $50\,\mathrm{GeV}/c^2$ (point labelled A in the figure); the slepton searches increase the limit to $76\,\mathrm{GeV}/c^2$ (point A$'$); with the Higgs boson searches included, the lower limit on $m_{1/2}$ is finally set to $90\,\mathrm{GeV}/c^2$ (point A$''$). For negative μ and $\tan\beta$ up to 4.6, the Higgs boson searches improve the lower limit on $m_{1/2}$ set by chargino and slepton searches alone.

From these studies, constraints on the mass of the lightest neutralino are derived. The lower limit on m_χ as a function of $\tan\beta$ is shown in Fig. 19 for $A_0 = 0$ and for both $\mu < 0$ and $\mu > 0$. Values of $\tan\beta$ lower than those displayed are unphysical in minimal supergravity for a top mass of $175\,\mathrm{GeV}/c^2$. There is little structure in the limit for $\mu > 0$. For $\mu < 0$, the limit is set at low $\tan\beta$ by the combination of Higgs boson and chargino searches. The limit degrades for $\tan\beta > 3.5$ because the exclusion domain from the Higgs boson searches no longer fully covers the corridor. For $\tan\beta > 5$, the limit improves again due to the increasing coverage of the corridor by the slepton searches. Altogether, a χ mass lower limit of $35\,\mathrm{GeV}/c^2$ is set for $A_0 = 0$. It is reached for $\tan\beta \sim 4.5$. It was verified that neutralino searches do not allow any improvement to be obtained at that point.

The impact of the value of A_0 chosen was also studied, and configurations were found for which χ mass values substantially lower than $35\,\mathrm{GeV}/c^2$ are allowed. An example of

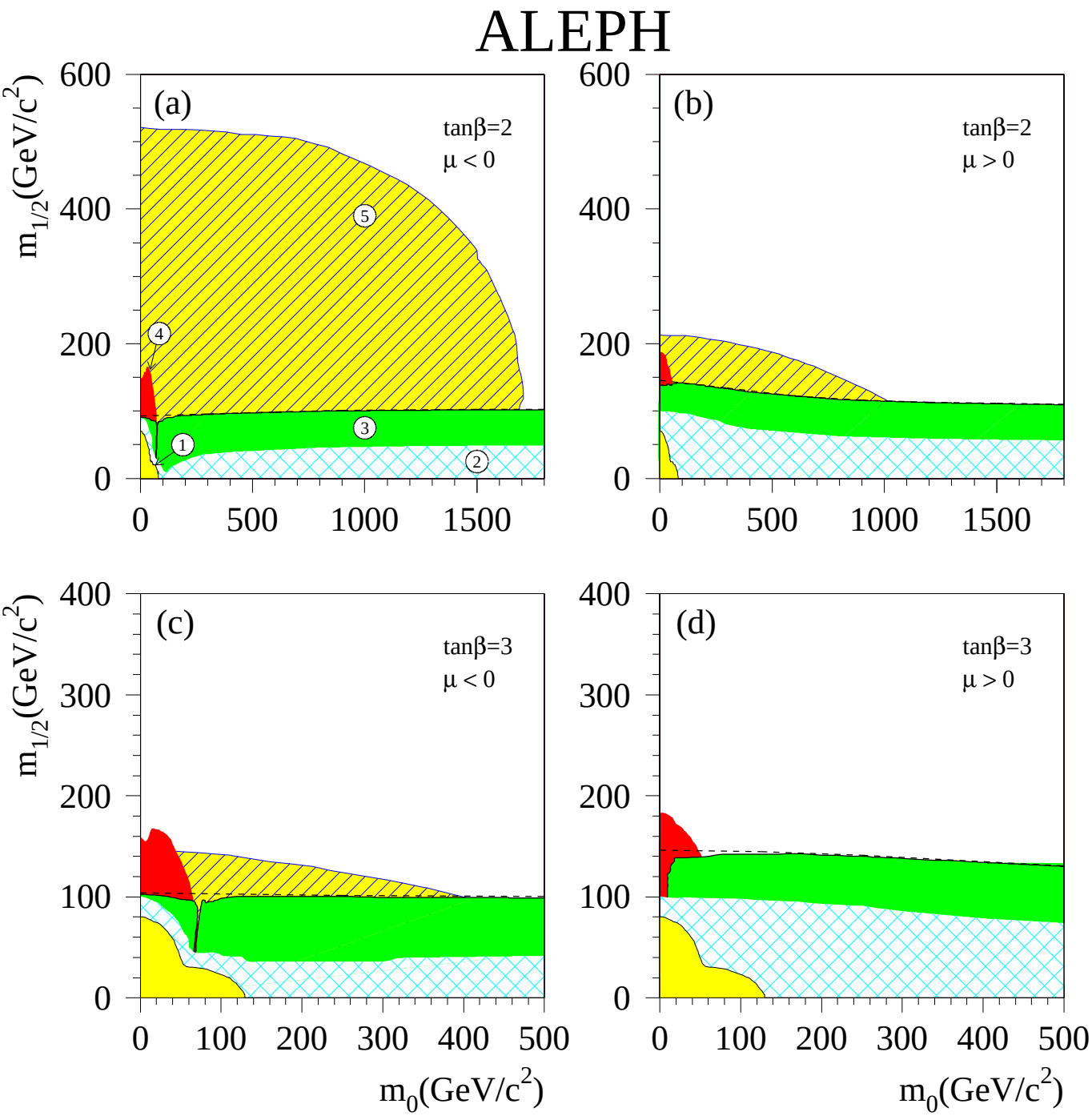

Figure 16: *Minimal supergravity scenario: domains of the $(m_0, m_{1/2})$ plane excluded for $\tan\beta = 2$ and 3, and for $A_0 = 0$. Region 1 is theoretically forbidden. The other regions are excluded by the Z width measurement at LEP1 (2), chargino (3) and slepton (4) searches, and by Higgs boson searches (5). The dashed lines represent the kinematic limit for direct chargino searches.*

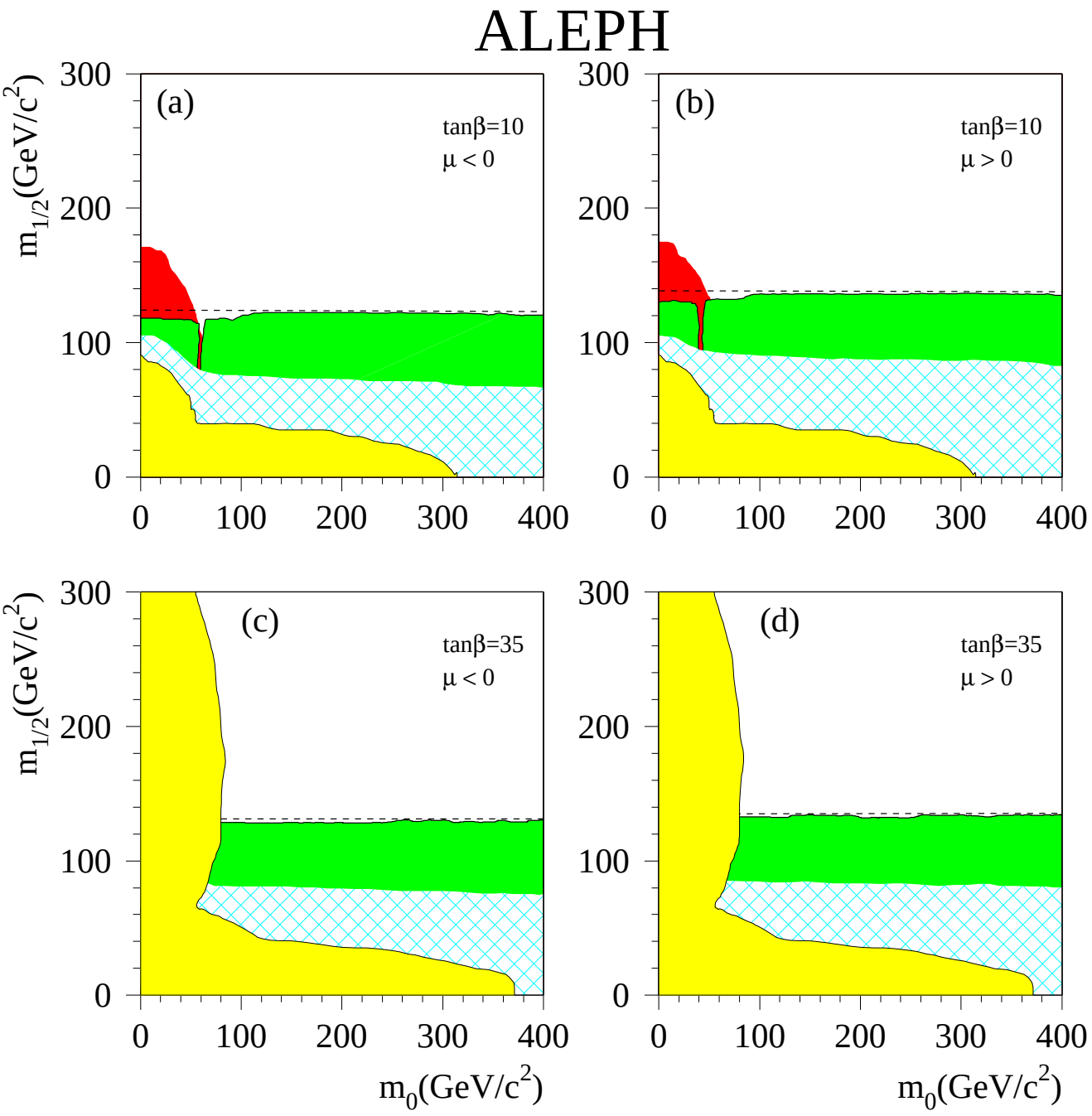

Figure 17: *Minimal supergravity scenario: domains of the* $(m_0, m_{1/2})$ *plane excluded for* $\tan\beta$*=10 and 35, and for* $A_0 = 0$*. The regions are defined as in Fig. 16.*

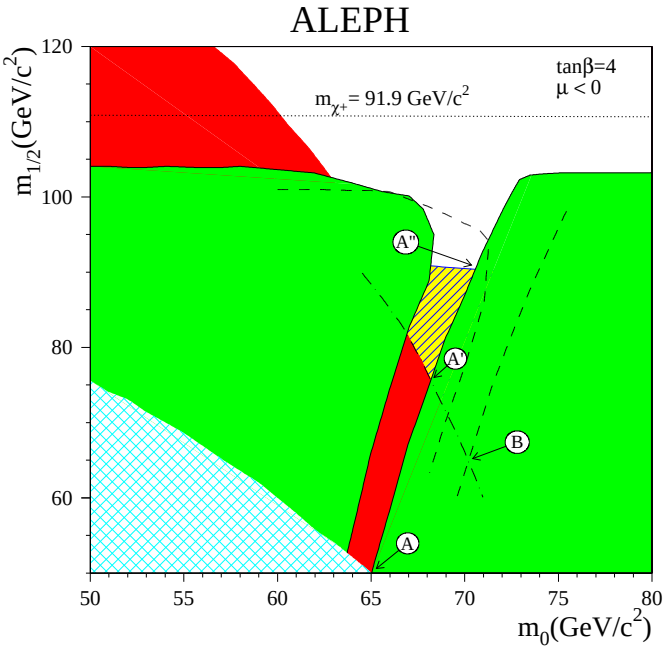

Figure 18: *Minimal supergravity scenario: zoom on the corridor in the $(m_0, m_{1/2})$ plane for $\tan\beta = 4$ and $\mu < 0$, and for $A_0 = 0$. The regions are defined as in Fig. 16. The points labelled A, A′, and A″ indicate the locations where the limits on $m_{1/2}$ are set set if only the Z width measurement and the chargino searches are used, if the slepton searches are used in addition, and with the inclusion of Higgs boson searches, respectively. The case $A_0 = -230$ GeV/c^2 is indicated by the dashed lines, and the corresponding $m_{1/2}$ limit is located at the point labelled B.*

such a configuration is illustrated in Fig. 18 for $\tan\beta = 4$, $\mu < 0$ and $A_0 = -230\,\mathrm{GeV}/c^2$. The lower limit on $m_{1/2}$, set at $65\,\mathrm{GeV}/c^2$ by chargino and slepton searches (point B) and corresponding to a χ mass of $29\,\mathrm{GeV}/c^2$, is not improved by the Higgs boson searches. The additional constraints of minimal supergravity therefore do not translate into a substantial improvement of the absolute χ mass lower limit.

5 Summary and conclusions

Searches for signals of the production of charginos and neutralinos in e^+e^- interactions have been carried out using the $57\,\mathrm{pb}^{-1}$ collected in 1997 by the ALEPH detector at centre-of-mass energies close to 183 GeV. Selections addressing the various topologies which may arise from chargino or neutralino production have been either updated from those which had been applied to the data collected at lower centre-of-mass energies [4] or newly developed. In all cases, the numbers and characteristics of the selected candidate events are consistent with the expectations from standard model processes.

Upper limits have been derived for the production cross sections of charginos and neutralinos. These are shown in Figs. 3 and 4 for $e^+e^- \to \chi^+\chi^-$ and $e^+e^- \to \chi\chi'$. In these figures, the assumption is made that the $\chi^\pm$ and χ' decays proceed via virtual W and Z exchanges. They can otherwise be regarded as practically model independent.

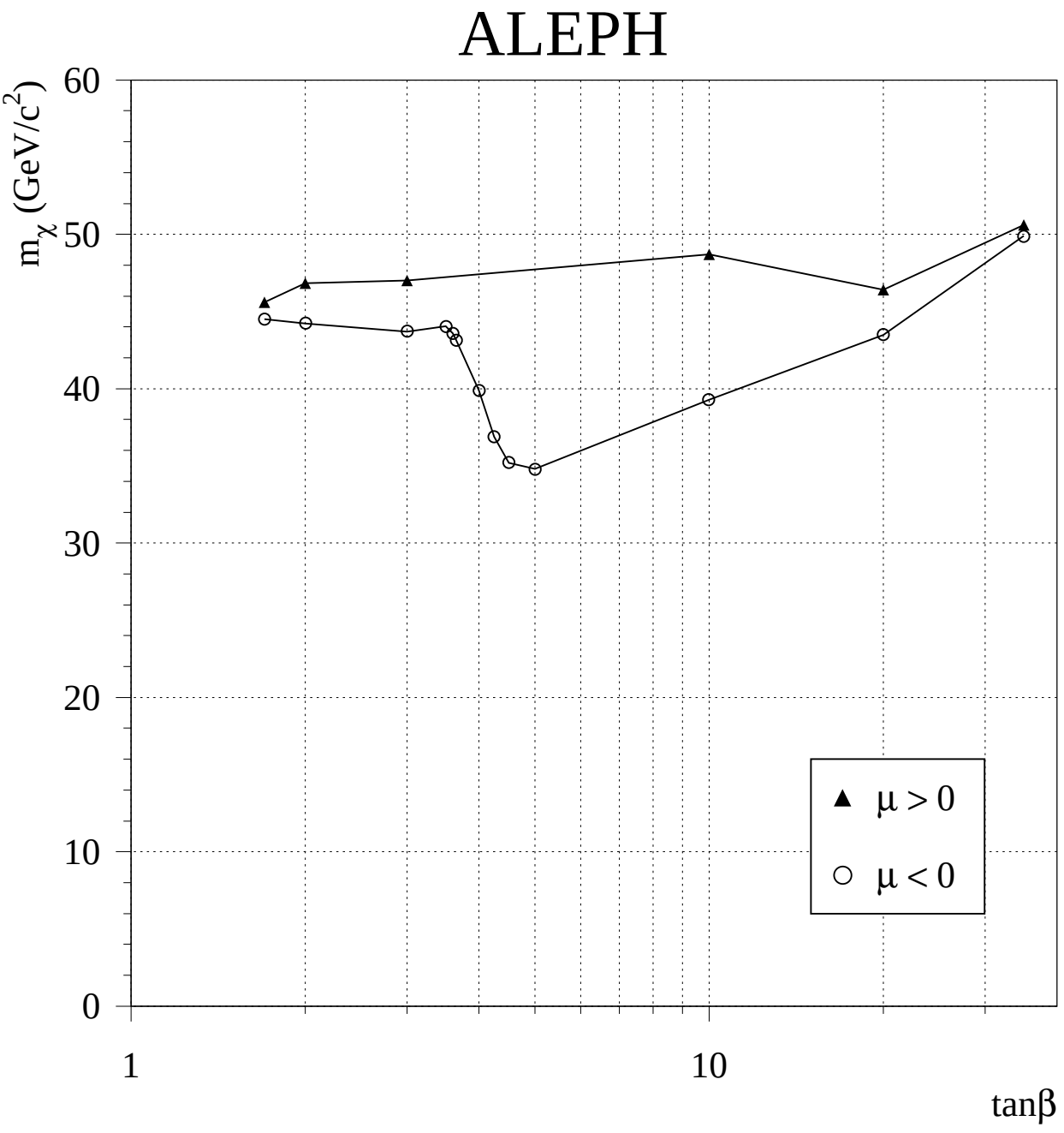

Figure 19: *In the minimal supergravity scenario, χ mass lower limit as a function of tan β for $A_0 = 0$ and for $\mu < 0$ (circles) and $\mu > 0$ (triangles).*

In the framework of the MSSM with gaugino mass unification, these cross section limits can be turned into excluded domains in the MSSM parameter space or into chargino and neutralino mass lower limits, assuming all sfermions to be heavy. Such excluded regions in the (μ, M_2) plane are shown in Figs. 5 and 6 for $\tan\beta = \sqrt{2}$ and 35. These results can equivalently be viewed as chargino or neutralino mass limits, as depicted in Figs. 7 and 8 for $\tan\beta = \sqrt{2}$. The exclusions extend very close to the kinematic limit, at least as long as the mass difference $m_{\chi^\pm} - m_\chi$ or $m_{\chi'} - m_\chi$ is not too small.

The interpretation of the results for lower scalar masses has been performed in a more constrained version of the MSSM, inspired by supergravity models. All slepton and squark masses are assumed to derive from a common scalar mass m_0 at the scale of grand unification, which correlates all chargino and neutralino production cross sections and decay branching ratios. (The impact of mixing, previously shown to be small [4], has been neglected.) For low m_0 values, which lead to a reduced sensitivity of chargino searches, advantage can be taken of the results of the slepton searches [2] which can be interpreted in terms of the same MSSM parameters with no further assumption. The interplay of the various constraints is demonstrated in Fig. 13 for $m_0 = 75\,\mathrm{GeV}/c^2$ and $\tan\beta = \sqrt{2}$.

The searches for the MSSM Higgs bosons [5] can also be used to constrain the MSSM parameter space, at least for low values of $\tan\beta$. Since the Higgs boson masses depend on the stop sector through radiative corrections, results from searches for stops [3] must also be used. In the derivation of the exclusion domains, unification of scalar quark and lepton masses is therefore an essential ingredient. Since stop mixing also influences the Higgs sector, the A_t parameter is left free in order to produce the most general results. As shown in Fig. 15, a substantial extension of the excluded region for $m_0 = 75\,\mathrm{GeV}/c^2$ and $\tan\beta = \sqrt{2}$ is obtained.

The model commonly referred to as minimal supergravity further assumes that all scalar masses, including those pertaining to the Higgs sector, are unified. This renders the results from Higgs boson searches even more constraining. Moreover, electroweak symmetry breaking is induced dynamically, thus allowing the μ parameter to be calculated except for a sign ambiguity. In addition, all trilinear couplings such as A_t are assumed to derive from a common value A_0 at GUT scale. Results obtained in this highly constrained model are presented in Figs. 16 and 17 where exclusion domains in the $(m_0, m_{1/2})$ plane are shown for $A_0 = 0$ and for several values of $\tan\beta$.

In the various scenarios considered above, the excluded regions can be turned into lower limits for the mass m_χ of the lightest neutralino, as summarized below.

- In the MSSM with gaugino mass unification, the searches for charginos reported in this paper allow a χ mass limit as a function of $\tan\beta$ to be obtained for large slepton masses, as shown in Fig. 11. For $m_0 > 500\,\mathrm{GeV}/c^2$, the $\tan\beta$ independent lower limit on m_χ is $29\,\mathrm{GeV}/c^2$, and is reached for $\tan\beta = 1$.

- The evolution of the limit on m_χ as a function of m_0 and $\tan\beta$ has been determined, under the assumption of slepton and squark mass universality, and using the results from neutralino and slepton searches in addition. Examples of results are shown in

Fig. 14. From these studies, it is concluded that the χ mass exceeds $28\,\mathrm{GeV}/c^2$ for any m_0 when $\tan\beta < 6$. The $\tan\beta$ and m_0 independent lower limit on m_χ is $27\,\mathrm{GeV}/c^2$. It is reached in the gaugino region for large $\tan\beta$, when charginos and sneutrinos are mass degenerate.

- The Higgs boson and stop searches allow the χ mass lower limit to be improved for low $\tan\beta$ and low m_0 as shown in Fig. 14.

- In minimal supergravity, *i.e.*, with unification of all scalar masses and with radiative electroweak symmetry breaking, the χ mass is further constrained, as shown in Fig. 19 for $A_0 = 0$. For this particular choice of A_0, the lower limit on m_χ is $35\,\mathrm{GeV}/c^2$, independent of m_0 and $\tan\beta$. However, the A_0 independent limit is not larger than 29 GeV/c^2.

The limits on chargino and neutralino masses and the constraints on the parameter space of the MSSM reported in this paper are significantly better than the results obtained at lower energies by ALEPH [4, 22] and by the other LEP experiments [32]. In particular, the χ mass lower limit is increased up to $27\,\mathrm{GeV}/c^2$. The DELPHI [33] and OPAL [34] collaborations recently reported results of their searches for charginos and neutralinos in their 183 GeV data. In Ref. [33], only the case of heavy sfermions is considered; the χ mass lower limit set in Ref. [34] is $24\,\mathrm{GeV}/c^2$.

For the first time, constraints on the MSSM parameters have been inferred from searches for Higgs bosons. At LEP, an interpretation within the framework of minimal supergravity has up to now been performed only by ALEPH.

Acknowledgements

We wish to congratulate our colleagues from the accelerator divisions for the very successful operation of LEP at high energy. We are indebted to the engineers and technicians in all our institutions for their contribution to the excellent performance of ALEPH. Those of us from nonmember countries thank CERN for its hospitality.

Appendix A: Selection variables

The variables used in the chargino and neutralino selections are described below. All variables are calculated using energy flow particles. They are separated into five categories: variables linked to the global event properties, to the event separation into hemispheres, to the jet reconstruction, to the kinematic reconstruction of $\gamma\gamma \to$ hadrons events and to the presence of an identified lepton.

Global event properties

The visible mass $M_{\rm vis}$, and energy $E_{\rm vis}$, the missing mass $M_{\rm miss}$ and transverse momentum P_T as well as the number of good tracks $N_{\rm ch}$ are important tools to separate the signals from standard processes and are correlated with the mass difference ΔM. Good tracks are charged particle tracks with at least four hits in the TPC originating from within a cylinder of radius 2 cm and length 20 cm centered on the interaction point.

The missing momentum polar and azimuthal angles, $\theta_{\rm miss}$ and $\phi_{\rm miss}$, are used to reject events with energy lost along the beam axis or in cracks. In particular, there are small vertical regions of reduced sensitivity between the modules of the luminosity calorimeter. Most selections use tighter cuts when the missing momentum azimuthal direction is compatible with the vertical direction.

The amount of energy $E_{\rm w}^{30}$ detected in a 30° wedge around the missing momentum (in the plane transverse to the beam axis) is a measurement of the isolation of the missing momentum. Although there are neutrinos in τ decays or heavy quark semileptonic decays, they are not in general isolated in this respect. Since there might also be energy lost along the beam direction (*e.g.*, photons from radiative return to the Z resonance), only the transverse plane is considered.

The energy E_{12} detected within 12° of the beam axis is useful to reduce the $\gamma\gamma$ background. The fraction F_{30° of the visible energy within 30° of the beam axis is a measure of the centrality of the event.

The presence of an isolated high energy photon is indicative of a radiative return to the Z resonance. A photon is isolated if no energy flow particle is detected in a 30° half-angle cone around its direction, excluding an inner cone of 5° half-angle to allow for shower split-off. Only photons of energy in excess of 10 GeV are considered.

In the energy flow algorithm, neutral hadrons arise from energy deposits not compatible with the interaction of charged particles and not identified as photons. This class of objects is sensitive to hadronic shower fluctuations. Fake neutral hadrons might spoil the event kinematics, especially in the case of low visible energy events like $\gamma\gamma$ events. The energy from neutral hadrons $E_{\rm nh}$ (or the fraction $F_{\rm nh} = E_{\rm nh}/E_{\rm vis}$) and the missing transverse momentum computed excluding neutral hadrons $P_T^{\overline{\rm nh}}$ are used to reject this type of events.

Hemisphere properties

The thrust axis is used to separate events into two hemispheres. Its polar angle θ_T is a measure of the centrality of the event. The acoplanarity $\Delta\Phi$ is the angle between the hemisphere momenta, and the inverse boost ($\mathcal{B} = \sqrt{(1/\gamma_1^2 + 1/\gamma_2^2)/2}$, where $\gamma_i = E_i/m_i$) measures the mean boost of the hemispheres. The transverse acoplanarity $\Delta\Phi_T$ is defined similarly to $\Delta\Phi$ but, before calculating the thrust axis, by projecting the event onto the plane transverse to the beam axis.

Jet properties

The definition of hemispheres using the thrust axis is sensitive to the boost of the event and may not be appropriate, *e.g.*, for $\gamma\gamma$ events. As an alternative, the event is forced to form two jets with the Durham algorithm and similar quantities are calculated, in particular the jet masses $M_{\mathrm{j1,j2}}$ and polar angles $\cos\theta_{\mathrm{j1,j2}}$.

The y_{cut} values y_{23} and y_{34} for which an event clustered with the Durham algorithm changes from a two- to a three-jet, and from a three- to a four-jet topology, are used to characterize multi-jet events and help reject the $\mathrm{q\overline{q}}$ and WW backgrounds.

Kinematic reconstruction of $\gamma\gamma \to$ hadrons

With the hypothesis that the kinematics of the event is that of a $\gamma\gamma$ interaction with the outgoing electron (positron) undeflected, it is possible to reconstruct the four-momentum of the deflected positron (electron). If the smaller polar angle θ_{scat} of the two hypotheses is large, the outgoing particle should be detected in $\gamma\gamma$ events. If not, its energy might have been poorly reconstructed, *e.g.*, due to cracks. The minimal angle θ_{point} of the reconstructed outgoing particle with any energy flow object is used to reject this type of events.

Leptons

The presence of an identified electron or muon is a powerful tool to reduce background for the relevant chargino and neutralino topologies. The energy $E_{\ell 1}$ of the leading lepton and its isolation $E_{\ell 1}^{30}$ (calculated as the energy in a cone of 30° half-angle, excluding neutral energy flow particles in a 5° half-angle cone) and its transverse momentum $P_{T_{\ell 1}}$ allow signal and backgrounds to be separated. The mass M_{had} and energy E_{had} of the recoiling system are used to reject the WW background. The acoplanarity between the lepton and the recoiling system is denoted $\Delta\Phi_{\ell \mathrm{h}}$. In events with several leptons, the energy of the next-to-leading lepton $E_{\ell 2}$ is used to separate primary leptons from secondary leptons or electrons from photon conversions.

Appendix B: Selection criteria

The anti-$\gamma\gamma$ cuts for the chargino 4J and 2Jℓ selections are given in Table 5 and those for the neutralino AJ and Mℓ selections in Table 6.

The other selection criteria are given in

- Table 7 for the 4J and 2Jℓ selections for high and low ΔM;
- Table 8 for the 4J and 2Jℓ selections for very low ΔM;
- Table 9 for the 2Jτ selections;
- Table 10 for the Aℓ-3 selection;
- Table 11 for the AJ and Mℓ selections.

The cuts for the Aℓ-χ selection are optimized in each point of the explored parameter space. Typical values for the cuts on the two leading lepton momenta are identical to those of the Mℓ selection given in Table 11.

Throughout the tables, energies are expressed in GeV, momenta in GeV/c and masses in GeV/c^2.

Table 5: *Cuts against $\gamma\gamma \to$ hadrons for the chargino 4J and 2Jℓ selections. The † indicates that the cut is applied when the azimuthal angle of the missing momentum is within 15° of the vertical plane. The 4J-L cuts are also used for the 2Jτ selections.*

Chargino - 4J		
	ΔM range	
	H	L
$M_{\rm vis}$	> 4	
$N_{\rm ch}$	≥ 7	≥ 4
$P_T \geq f_1\sqrt{s}$ / $f_2\sqrt{s}^{\dagger}$	$f_1 = 5\%,\ f_2 = 7.5\%$	
$\Delta\Phi_T$	$< 175°$	
E_{12}	$< 5\%\sqrt{s}$	$= 0$
$\theta_{\rm scat} > \theta_1$ or $\theta_{\rm point} > \theta_2$	$\theta_1 = 10°, \theta_2 = 15°$	$\theta_1 = 15°, \theta_2 = 10°$
$(\theta_{\rm scat} - 10°) > \theta_1$ or $\theta_{\rm point} > \theta_2$	$\theta_1 = 3°, \theta_2 = 5°$	–
$\lvert\cos\theta_{\rm miss}\rvert$	< 0.95	
$F_{\rm nh}$	$< 45\%$	
$F_{\rm nh} < f_1$ or $P_T^{\rm nh} > f_2\sqrt{s}$	$f_1 = 30\%, f_2 = 3\%$	
$E_{\ell 1}$	$< 20\%\sqrt{s}$	
thrust	< 0.9	–
$E_{\rm w}^{30}$	–	$< 1.5\%\sqrt{s}$

Chargino - 2Jℓ		
	ΔM range	
	H	L
$M_{\rm vis}$	> 4	
$N_{\rm ch}$	≥ 3	
identified lepton	$E_{\ell 1} > 2.5$	
$P_T \geq f_1\sqrt{s}$ / $f_2\sqrt{s}^{\dagger}$	$f_1 = 5\%,\ f_2 = 7.5\%$	$f_1 = 2.5\%,\ f_2 = 3.75\%$
$\Delta\Phi_T$	$< 175°$	
E_{12}	$< 5\%\sqrt{s}$	$= 0$
$\theta_{\rm scat} > \theta_1$ or $\theta_{\rm point} > \theta_2$	$\theta_1 = 15°, \theta_2 = 5°$	
$\lvert\cos\theta_{\rm miss}\rvert$	–	< 0.95
$F_{\rm nh}$	$< 45\%$	
$\min(E_{\rm w}^{30}, E_{\ell 1}^{30})$	–	$< 0.5\%\sqrt{s}$
$E_{\ell 1}$	$< 30\%\sqrt{s}$	$< 20\%\sqrt{s}$
$M_{\rm miss}$	$> 25\%\sqrt{s}$	–

Table 6: *Cuts against $\gamma\gamma \to$ hadrons for the neutralino AJ and Mℓ selections. The † indicates that the cut is applied when the azimuthal angle of the missing momentum is within 15° of the vertical plane.*

Neutralino - AJ		
	ΔM range	
	H	L
$M_{\rm vis}$	> 4	
$N_{\rm ch}$	≥ 7	≥ 4
$P_T \geq f_1\sqrt{s}$ / $f_2\sqrt{s}^{\dagger}$	$f_1 = 5\%,\ f_2 = 7.5\%$	$f_1 = 3\%,\ f_2 = 4.5\%$
$P_T/E_{\rm vis}$	$> 20\%$	$> 40\%$
$\Delta\Phi_T$	$< 170°$	$< 120°$
$\Delta\Phi$	$< 170°$	–
E_{12}	$< 5\%\sqrt{s}$	$= 0$
$\theta_{\rm scat} > \theta_1$ or $\theta_{\rm point} > \theta_2$	$\theta_1 = 15°, \theta_2 = 5°$	
$\lvert\cos\theta_{\rm miss}\rvert$	< 0.95	
$F_{\rm nh}$	$< 45\%$	
$F_{\rm nh} < f_1$ or $P_T^{\overline{\rm nh}} > f_2\sqrt{s}$	$f_1 = 30\%$	
	$f_2 = 3\%$	$f_2 = 1.8\%$
$E_{\ell 1}$	$< 20\%\sqrt{s}$	
$E_{\rm w}^{30}$	$< 7.5\%\sqrt{s}$	$= 0$
$F_{30°}$	$< 70\%$	–

Neutralino - Mℓ	
$M_{\rm vis}$	> 4 and trigger conditions
$P_T \geq f_1\sqrt{s}$ / $f_2\sqrt{s}^{\dagger}$	$f_1 = 5\%,\ f_2 = 7.5\%$
$\Delta\Phi_T$	$< 175°$
E_{12}	$< 5\%\sqrt{s}$
$\theta_{\rm scat} > \theta_1$ or $\theta_{\rm point} > \theta_2$	$\theta_1 = 15°, \theta_2 = 5°$
$\lvert\cos\theta_{\rm miss}\rvert$	< 0.95
$F_{\rm nh}$	$< 45\%$
$F_{\rm nh} < f_1$ or $P_T^{\overline{\rm nh}} > f_2\sqrt{s}$	$f_1 = 30\%, f_2 = 3\%$

Table 7: *Cut values for the chargino 4J and 2Jℓ selections for the high and low ΔM regions.*

Chargino - 4J		
	ΔM range	
	H	L
anti-$\gamma\gamma$ cuts	Yes	
thrust	< 0.9	$< 0.95 - 0.0025\Delta M$
$E_{\rm vis}$	$< 8 + 2.35\Delta M - 0.017\Delta M^2$	–
y_{23}	$> -0.055 + 0.002\min(\Delta M, 40)$	–
$y_{23} > y_1(M_{\rm vis} - 60)$	$y_1 = 0.0005[10 + \max(\Delta M - 45, 0)]$	–
$E_{\rm w}^{30}$	$< 8\%\sqrt{s}$	–
$E_{\ell 1}$	–	< 20
$\mathcal{B}$	–	$> 0.01\Delta M$
$M_{\rm miss}$	–	$M_{\rm miss} > (176 - 2\Delta M)$ $M_{\rm miss} < (185 - 1.5\Delta M)$
$M_{\rm vis}$	–	$(-28 + 1.8\Delta M) < M_{\rm vis} < 75$
Isolated γ	none	

Chargino - 2Jℓ		
	ΔM range	
	H	L
anti-$\gamma\gamma$ cuts	Yes	
$N_{\rm ch}$	≥ 7 ($\Delta M > 22$) ≥ 5 ($\Delta M < 22$)	–
$E_{\ell 1}$	$< 20\%\sqrt{s}$ ($\Delta M < 70$) $< 25\%\sqrt{s}$ ($\Delta M > 70$)	< 20
$E_{\ell 1}$	$> 7\%\sqrt{s}$ ($\Delta M > 70$) $> 0.001\Delta M\sqrt{s}$ ($31 < \Delta M < 70$) $> 1\%\sqrt{s}$ ($\Delta M < 31$)	–
$E_{\ell 1}^{30}$	$< 15\%\sqrt{s}$	–
$E_{\ell 1}^{30} < f_1\sqrt{s}$ or $E_{\rm w}^{30} < f_2\sqrt{s}$	$f_1 = 2\%$, $f_2 = 5\%$	–
$E_{\rm had} < E_1$ or $E_{\ell 1} < E_2$	$E_1 = 55$, $E_2 = 17.5\%\sqrt{s}$	–
$y_{23} > y_1(E_{\rm had} - E_{\rm h})$	$y_1 = 0.05$ ($\Delta M > 70$) $y_1 = 1$ ($\Delta M < 70$)	–
	$E_h = 60$ ($\Delta M > 70$) $E_{\rm h} = 27.5 + 0.5\Delta M$ ($31 < \Delta M < 70$) $E_{\rm h} = 40$ ($\Delta M < 31$)	
$M_{\rm miss}$	> 56 ($\Delta M > 70$) $> 184.3 - 1.83\Delta M$ ($\Delta M < 70$)	$> (177 - 1.7\Delta M)$ $< (182 - 0.7\Delta M)$
thrust	–	$< 1.05 - 0.004\Delta M$
$\Delta\Phi_T$	–	$< 170^\circ$ ($< 130^\circ$ if $N_{\rm ch} \leq 4$)
$M_{\rm had}$	–	> 1.5

Table 8: *Cut values for the chargino 4J and 2Jℓ selections for the very low ΔM region. In the case of 4J-VL, the cuts are given for the ΔM region where the selection applies.*

Chargino - VL		
	Topology	
	4J	2Jℓ
$M_{\rm vis}$	> 3 and trigger conditions	
$N_{\rm ch}$	> 3	> 2
E_{12}	$= 0$	
$\theta_{\rm scat}$	$> \max(13, 38 - 2.5\Delta M)^\circ$	–
$\phi_{\rm miss}$	15° away from vertical plane	–
$\lvert\cos\theta_{\rm miss}\rvert$	< 0.92	< 0.9
$\cos\theta_{\rm j1,j2}$	< 0.9	< 0.94
thrust	< 0.85	< 0.9
$M_{\rm miss}$	$> 1.7E_{\rm vis}$	$> \max(120, 177 - 1,7\Delta M)$ $< (182 - 0.7\Delta M)$
$P_T/\sqrt{s}$	$> 2.3\%$ $> (7.4 + 1.6\Delta M)/600$ $< (4\Delta M + 20)/600$	1.7% (2.55%)†
$P_T/E_{\rm vis}$	$> 31\%$ or $P_T > 3\%\sqrt{s}$	$> 25\%$
$\Delta\Phi_T$	$< (110 + 5\Delta M)^\circ$ $< (2545P_T/\sqrt{s} + 50.5)^\circ$	$< 150^\circ$ if $N_{\rm ch} = 4$ $< 135^\circ$ if $N_{\rm ch} = 3$ and $\lvert\cos\theta_{\rm miss}\rvert > 0.7$
$F_{\rm nh}$	$< 40\%$ $= 0$ or $P_T^{\overline{\rm nh}} > 2\%\sqrt{s}$	–
jets	$(M_{\rm j1} + M_{\rm j2}) > 0.3M_{\rm vis}$ or $\lvert M_{\rm j1} - M_{\rm j2}\rvert > 0.2M_{\rm vis}$	–
$E_{\ell 1}$	< 10	> 1.2 (e), > 2.2 (μ)
$P_{T_{\ell 1}}$	–	> 1 > 2.5 or $\theta_{\rm scat} > 2^\circ$
$E_{\ell 1}^{30}$	–	< 8 $= 0$ or $\Delta\Phi_{\ell \rm h} < 100^\circ$
$E_{\rm w}^{30}$	–	$= 0$
$M_{\rm had}$	–	$\min(3, 1 + 0.1\Delta M) < M_{\rm had} < 30$

Table 9: *Cut values for the chargino 2Jτ selections for the very high, high and low ΔM regions.*

Chargino - 2Jτ			
	ΔM range		
	VH	H	L
anti-$\gamma\gamma$ cuts	Yes (4J-L)		
$M_{\rm miss}$	> 95	$> 160 - \Delta M$	$> 190 - 2\Delta M$
$M_{\rm miss}$	< 135	$< 182.5 - 0.75\Delta M$	$< 190 - \Delta M$
$M_{\rm vis}$	< 65	$< \Delta M + 5$	–
thrust	< 0.875	$< 1.025 - 0.0025\Delta M$	< 0.95
$-\log(y_{23})$	< 2.25	< 2.8	< 2.5
$E_{\ell 1}$	$< 5\%\sqrt{s}$		–
$\cos\theta_T$	–	< 0.95	
$\Delta\Phi_T$	–	$< 160^\circ$	$< 140^\circ$
$E_{\rm vis}$	–	$< 35\%\sqrt{s}$	–

Table 10: *Cuts on the energy of the leading lepton for the chargino Aℓ-3 selection.*

Chargino - Aℓ-3	
ΔM range	$E_{\ell 1}/E_{\rm beam} <$
$\Delta M > 15$	$0.074 + 0.00526\Delta M$
$7 < \Delta M < 15$	$0.014 + 0.00937\Delta M$
$\Delta M < 7$	$-0.0096 + 0.01049\Delta M$

Table 11: *Cuts for neutralino selections. The positions of the cuts for variables with a † depend on the point in the SUSY parameter space; typical values are given for illustration.*

Neutralino			
	Topology		
	AJ-H	AJ-L	4Jγ
anti-$\gamma\gamma$ cuts	Yes	Yes	Yes (4J-H)
$M^{\dagger}_{\rm miss}$	$> 174 - 1.06\Delta M$		110
thrust	< 0.95		–
$\Delta\Phi$	$< 170^{\circ}$	–	$< 160^{\circ}$
$\Delta\Phi_T$	$< 170^{\circ}$	–	
$E^{30}_{\rm w}$	–		$< 7.5\%\sqrt{s}$
isolated γ	–		1

	Topology		
	AJ-H	AJ-L	4Jγ
anti-$\gamma\gamma$ cuts	Yes		
identified e/μ	$\geq$ 2e or $\geq 2\mu$		
$E_{\ell 1}{}^{\dagger}$	< 60		
$E_{\ell 2}{}^{\dagger}$	< 25 if no isolated γ		
$M^{\dagger}_{\rm vis}$	< 60		

References

[1] H.E. Haber and G.L. Kane, Phys. Rep. **117** (1985) 76;
R. Barbieri, Riv. Nuovo Cim. **11** No. 4 (1988) 1.

[2] ALEPH Coll., *"Search for sleptons in e^+e^- collisions at centre-of-mass energies up to 184 GeV"*, Phys. Lett. **B433** (1998) 176.

[3] ALEPH Coll., *"Scalar quark searches in e^+e^- collisions at $\sqrt{s}$ =181−184* GeV", Phys. Lett. **B434** (1998) 189.

[4] ALEPH Coll., *"Searches for Charginos and Neutralinos in e^+e^- Collisions at $\sqrt{s}$ = 161 and 172 GeV"*, Euro. Phys. J. **C2** (1998) 3.

[5] ALEPH Coll., *"Searches for the neutral higgs bosons of the MSSM in e^+e^- collisions at centre-of-mass energies of 181−184 GeV"*, CERN-EP/98-145, to be published in Phys. Lett. **B**.

[6] H.P. Nilles, Phys. Rep. **110** (1984) 1.

[7] ALEPH Coll., *"ALEPH: a detector for electron-positron annihilations at LEP"*, Nucl. Instrum. and Methods **A294** (1990) 121.

[8] D. Creanza *et al.*, *"The new ALEPH silicon vertex detector"*, Nucl. Instrum. and Methods **A409** (1998) 157.

[9] ALEPH Coll., *"Performance of the ALEPH detector at LEP"*, Nucl. Instrum. and Methods **A360** (1995) 481.

[10] J.-F. Grivaz and F. Le Diberder, *"Complementary analyses and acceptance optimization in new particle searches"*, LAL-92-37 (1992).

[11] S. Katsanevas and P. Morawitz, Comp. Phys. Commun. **112** (1998) 227.

[12] H. Anlauf *et al.*, Comp. Phys. Commun. **79** (1994) 466.

[13] S. Jadach *et al.*, Comp. Phys. Commun. **36** (1985) 191.

[14] J.A.M. Vermaseren in *Proceedings of the IVth international Workshop on Gamma Gamma Interactions*, Eds G. Cochard, and P. Kessler, Springer Verlag, 1980;
ALEPH Coll., "*An experimental study of $\gamma\gamma \to$ hadrons at LEP*",
Phys. Lett. **B313** (1993) 509.

[15] R. Engel, Z. Phys. **C66** (1995) 203;
R. Engel and J. Ranft, Phys. Rev. **D54** (1996) 4144.

[16] M. Skrzypek, S. Jadach, W. Placzek, and Z. Was, Comp. Phys. Commun. **94** (1996) 216.

[17] T. Sjöstrand, Comp. Phys. Commun. **82** (1994) 74; CERN-TH 7112/93 (1993, revised August 1994).

[18] R.D. Cousins and W.L. Highland, Nucl. Instrum. and Methods **A320** (1992) 331.

[19] The LEP Collaborations ALEPH, DELPHI, L3, OPAL, the LEP Electroweak Working Group, and the SLD Heavy Flavour Group, *"A Combination of Preliminary Electroweak Measurements and Constraints on the Standard Model"*, CERN-PPE/97-154.

[20] ALEPH Coll., *"Searches for new particles in Z decays using the ALEPH detector"*, Phys. Rep. **216** (1992) 253.

[21] ALEPH Coll., *"Mass limit for the lightest neutralino"*, Z. Phys. **C72** (1996) 549.

[22] ALEPH Coll., *"Update of the mass limit for the lightest neutralino"*, contribution #594 to the IECHEP, Jerusalem, August 1997.

[23] CDF Coll., *"Search for Gluinos and Squarks at the Fermilab Tevatron Collider"*, Phys. Rev. **D56**, Rapid Communications, R1357 (1997).

[24] R. Barbieri and M. Frigeni, Phys. Lett. **B258** (1991) 395.

[25] M. Carena, M. Quiros, and C. Wagner, Nucl. Phys. **B461** (1996) 407.

[26] W. de Boer *et al.*, Z. Phys. **C67** (1995) 647.

[27] ALEPH Coll., *"Search for the standard model Higgs boson at the LEP2 collider near* $\sqrt{s} = 183\,GeV$*"*, CERN-EP/98-144, to be published in Phys. Lett. **B**.

[28] ALEPH Coll., *"Search for invisible decays of the Higgs boson in* e^+e^- *collisions"*, contribution #617 to the IECHEP, Jerusalem, August 1997.

[29] ALEPH Coll., *"Search for charged Higgs bosons in* e^+e^- *collisions at centre-of-mass energies from 130 GeV to 172 GeV"*, Phys. Lett. **B418** (1998) 419.

[30] ALEPH Coll., *"Mass limit for the standard model Higgs boson with the full LEP1 ALEPH data sample"*, Phys. Lett. **B384** (1996) 427;
ALEPH Coll., *"Search for a non-minimal Higgs boson produced in the reaction* $e^+e^- \to hZ^*$*"*, Phys. Lett. **B313** (1993) 312.

[31] F.E. Paige, S.D. Protopopescu, H. Baer, and X. Tata, *"ISAJET 7.37- A Monte Carlo Event Generator for pp,* $p\bar{p}$ *and* e^+e^- *Reactions"*; documentation and code available from `ftp://penguin.phy.bnl.gov/pub/isajet/`.

[32] DELPHI Coll., *"Search for charginos, neutralinos and gravitinos at LEP"*, Eur. Phys. J. **C1** (1998) 1;
L3 Coll., *"Search for Scalar Leptons, Charginos and Neutralinos in* e^+e^- *collisions at* $\sqrt{s} = 161 - 172\ GeV$*"*, Eur. Phys. J. **C4** (1998) 207;
OPAL Coll., *"Search for Chargino and Neutralino Production at* $\sqrt{s}$ *=170 and 172 GeV at LEP"*, Eur. Phys. J. **C2** (1998) 213.

[33] DELPHI Coll., *"Search for charginos, neutralinos and gravitinos in* e^+e^- *interactions at* $\sqrt{s}$ *=183 GeV"*, CERN-EP/98-176, submitted to Phys. Lett. **B**.

[34] OPAL Coll., *"Search for Chargino and Neutralino Production at $\sqrt{s}$ =181−184 GeV at LEP"*, CERN-EP/98-136, submitted to Euro. Phys. J. **C**.